Critical Behavior and Crossover Scaling in Symmetric Polymer Mixtures: A Monte Carlo Investigation

H.-P. Deutsch and K. Binder*

Institut für Physik, Johannes Gutenberg-Universität Mainz, Staudinger Weg 7, W-6500 Mainz, Federal Republic of Germany

Received January 21, 1992; Revised Manuscript Received May 27, 1992

ABSTRACT: Symmetrical polymer A-polymer B mixtures (chain length $N_A = N_B = N$) are simulated by Monte Carlo methods, using the bond fluctuation model on simple cubic lattices, for $N = 16$ to $N = 256$ at a volume fraction of occupied lattice sites $\phi = 0.5$ (which corresponds to a dense melt). Applying recently developed efficient simulation techniques (grand-canonical sampling of the mixture thermodynamics is combined with multiple histogram data evaluation and finite size scaling techniques), very precise estimates of critical temperatures, phase diagrams, composition-dependent effective Flory-Huggins parameters, and, last but not least, critical exponents and amplitudes are obtained. The data provide clear evidence for a linear dependence of the critical temperature on chain length, $k_B T_c/\epsilon \approx 2.15N + 1.35$, and thus disagree with the integral equation theory prediction ($T_c \propto \sqrt{N}$) of Schweizer and Curro. Consistent with the work of Sariban and Binder, however, it is concluded that the naive application of Flory-Huggins theory would overestimate strongly the proportionality constant relating T_c with N. For the first time, clear evidence for a crossover from Ising-like critical behavior (dominating at small N) to mean-field critical behavior (which emerges in the limit $N \to \infty$) is seen in simulations, consistent with the Ginzburg criterion for polymer mixtures.

1. Introduction

About 50 years ago, Flory,[1] Huggins,[2] and others[3-9] proposed lattice models for the description of the thermodynamics of polymer mixing. With various crude but simple approximations, they obtained a mean-field-like theory of polymer mixtures, which is widely used in conjunction with practical applications of polymer blends and also serves as a very useful starting point for further theoretical developments. Such developments either attempt a more realistic description of the equation of state of the considered polymer[10-14] or consider inhomogeneous situations: interfaces,[15-18] wall effects,[19,20] block copolymer microphase separation,[21-29] spinodal decomposition of mixtures,[30-33] interdiffusion,[32,34-39] etc. Since the mean-field approximation for polymer blends can be justified with a Ginzburg-type self-consistency criterion,[9,32,40] one has believed that the widespread use of the Flory-Huggins theory is on safe grounds.

This belief has been called into question very recently by several different approaches: (i) Monte Carlo studies of the Flory-Huggins lattice model by Sariban and Binder,[41-43] which simulate exactly the basic lattice model but avoid other approximations such as the mean-field approximation, revealed surprisingly large discrepancies between the theory and the "computer experiment": the predicted critical temperatures were too high by a factor of at least 2 or 3; the critical behavior was Ising-like[44] instead of mean-field-like; if one tried to fit the Flory-Huggins equation of state[6] to the data, a spurious concentration dependence of the Flory-Huggins χ parameter was obtained. (ii) A "renormalization" of the effective Flory-Huggins χ parameter driving the unmixing was obtained by various analytical theories.[45-52] However, these theories consider different mechanisms, and it is not so clear how these effects act together and under what conditions these theories are valid: a reduction of χ due to excluded-volume effects (A-B contacts are avoided over the length scale of the "blob size" describing the screening of excluded-volume interactions[45,46]) should be important mainly for ternary blends (polymer A + polymer B + solvent), and this is consistent with simulations.[53,54] Another renormalization of χ due to density fluctuations should be small if the blend is nearly incompressible. The reduction of chain radii of gyration with increasing interaction strength seen first in the simulations[41,42,55] and later confirmed by analytical calculations[49] shows that the random-phase approximation[9] (RPA) is not accurate, and this fact clearly invalidates the mean-field theory to which the RPA is equivalent. However, a fully self-consistent theory of blends incorporating these deviations from the RPA remains to be given. A possible route to avoid RPA assumptions is the formulation of integral equation theories[51] but this approach may involve other problems, as discussed below. Still another interesting development is based on systematic improvements in the treatment of configurational entropies,[48] taking even special shapes of the monomers into account.

While all the theories characterized so far imply *quantitative* modifications of Flory-Huggins theory, Schweizer and Curro[50,51] in their integral equation theory even claim a dramatic qualitative failure of Flory-Huggins theory due to long-range correlation effects: while Flory-Huggins theory implies a linear relation between the critical temperature and chain length in the symmetric binary blend ($N_A = N_B = N$), ϵ being a microscopic pair interaction energy

$$k_B T_c/\epsilon \propto N \tag{1}$$

they predict in $d < 4$ space dimensions that[50,51]

$$k_B T_c/\epsilon \propto N^{(d-2)/2} \tag{2}$$

Equation 2 implies that in the 3-dimensional systems of practical interest Flory-Huggins theory, including all extensions[1-39] and modifications,[45-49] is qualitatively wrong!

Thus the theoretical understanding of polymer blends at present clearly is very unsatisfactory. Since real polymer blends are never exactly symmetric and it is not obvious how asymmetry in the size and shape of the monomers affects the theoretical predictions, it is not straightforward to settle these issues. It is hence clearly desirable to clarify the validity of the theories by computer simulation, since there it is easy to choose a strictly symmetric model.[41-43] While previous work[41-43] has clearly given some valuable insight already, it has not given conclusive answers on

0024-9297/92/2225-6214$03.00/0

questions such as the distinction between eqs 1 and 2, and also the crossover from Ising-like to mean-field-like critical behavior, which should occur as the chain length increases,[9,32,40] has not yet been seen: the available chain lengths ($N \leq 64$ for volume fraction $\phi = 0.4$ of occupied sites, $N \leq 32$ for $\phi = 0.8$)[42] simply were too short. Moreover, even though the finite-size scaling behavior of these systems was clearly consistent with Ising exponents, certain ratios of critical amplitudes which should be as universal as the exponents were far off the values of the 3d Ising universality class.

In the present paper, we hence reconsider these problems and extend the simulation work on blends up to much longer chains ($N \leq 256$), making use of several recent advances in the performance and analysis of such simulations:

(i) Using the bond fluctuation model,[56-60] it is possible to equilibrate[60] chain configurations for chain lengths of order $N = 200$, at a volume fraction $\phi = 0.5$ of occupied sites for which the screening length is a few lattice spacings only,[60] and hence the system represents a dense polymer melt very well. This is possible due to the availability of very efficient computer simulation algorithms[57,59,60] for this model, which are well suited for vector processors[57,59] or massively parallel computers.[60]

(ii) Using the so-called "histogram techniques" recently proposed for the study of critical phenomena in spin models,[61] a significantly more efficient analysis of the computer simulations is possible. The implementation of these methods for polymers, in conjunction with finite-size scaling[62-64] techniques, is described in more detail elsewhere.[65]

In section 2, we now summarize the main features of the model and the data analysis, while section 3 describes our results for critical temperatures,[66] phase diagrams, and effective Flory–Huggins parameters. Section 4 presents our findings on critical exponents and critical amplitudes and addresses the question of a crossover from Ising-like to mean-field-like critical behavior. Section 5 summarizes our results, briefly discusses pertinent experiments,[67-71] and gives an outlook for further work.

2. Model and Simulation Technique

In the present work we use $L \times L \times L$ simple cubic lattices with box linear dimensions L ranging from $L_{min} = 24$ to $L_{max} = 48$ (for $N = 16$), from $l_{min} = 24$ to $L_{max} = 56$ (for $N = 32$), from $L_{min} = 32$ to $L_{max} = 80$ (for $N = 64$), from $L_{min} = 48$ to $L_{max} = 80$ (for $N = 128$) and from $L_{min} = 64$ to $L_{max} = 112$ (for $N = 256$). For each chain length, at least three distinctly different choices of L are necessary for applying finite-size scaling techniques,[64,65] and the minimum size L_{min} was chosen such that the probability for a chain to overlap with its periodic images is negligibly small. Since each monomer in the bond fluctuation model[59] blocks a cube containing eight neighboring sites (Figure 1), the number n of chains in our systems hence is $n = \phi L^3/(8N)$. With $\phi \equiv \phi_A + \phi_B = 1 - \phi_V = 0.5$ we have thus for $L = L_{min}$ a number $n = 54$ (for $N = 16$) or $n = 64$ (for $N = 256$), while the largest systems contain always several hundred different chains.

An unmixing tendency between different types (A and B) of chains is introduced by pairwise interactions ϵ_{AA}, ϵ_{AB}, and ϵ_{BB} between the effective monomer pairs of types AA, AB, and BB. Since we wish to study a precisely symmetric model, we have to choose $\epsilon_{BB}/\epsilon_{AA} = 1$. One could consider a model with purely repulsive forces ($\epsilon_{AA} = \epsilon_{BB} = 0$, $\epsilon_{AB} > 0$) or with purely attractive forces ($\epsilon_{AB} = 0$, $\epsilon_{AA} = \epsilon_{BB} < 0$). Both cases have been considered in earlier work,[42] and it was found that for large ϕ there are only minor differences between these choices. In the present work we thus study a single, intermediate case, where all energy parameters are chosen equal in magnitude, $\epsilon_{AA} = \epsilon_{BB} = -\epsilon_{AB} = -\epsilon$.

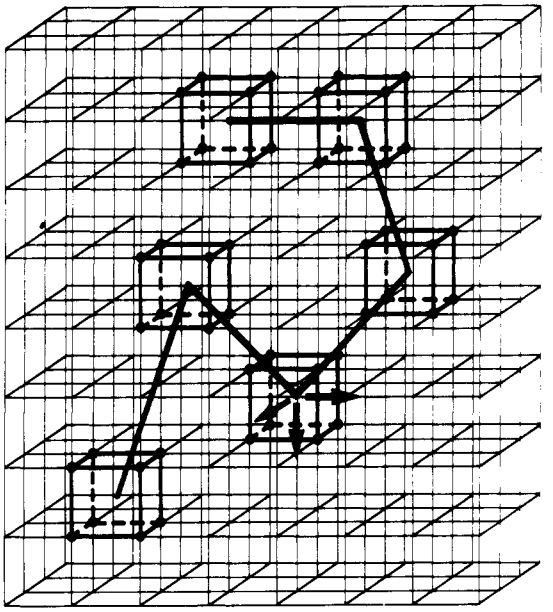

Figure 1. Schematic illustration of the bond fluctuation model. A monomer blocks a cube containing eight lattice sites for occupation by other monomers. The length b of the bonds connecting two neighboring cubes along the chain is restricted to one of the values $b = 2, \sqrt{5}, \sqrt{6}, 3$, or $\sqrt{10}$ (in units of the lattice spacing). Chain configurations relax by random diffusive hops of the monomers by one lattice spacing in either the $\pm x$, $\pm y$, or $\pm z$ direction. Such moves are acceptable only if they do not lead to any violation of the condition that each lattice site is occupied at most once and that the new bond vectors still belong to the allowed set.

A second choice has to be made concerning the range of the interaction. We apply the above energy $\pm\epsilon$ whenever a pair of monomers has the distance vector $P(2,0,0)$, $P(2,1,0)$, and $P(2,1,1)$, respectively. Here the symbol P denotes all permutations and sign combinations of the indices. This amounts of 54 choices in total. The range of interaction from 2 up to $\sqrt{6}$ is needed to fully include the contribution from the "nearest-neighbor" peak of the pair correlation function between monomers; see ref 59. A vectorized version of this algorithm implemented at a CRAY-YMP executes about 3×10^5 attempted monomer moves per second. Since our largest lattice contains 87 808 monomers, an attempt per monomer taking 0.3 s, at least on the order of N^2 attempted moves per monomer are necessary to generate a configuration of the chains that is statistically uncorrelated from the previous configuration, it is obvious that such simulations are very difficult and time-consuming even for supercomputers.

As in previous work,[41-43] the simulation is carried out in the grand-canonical ensemble of the mixture. Thus the chemical potential difference per monomer $\Delta\mu \equiv \mu_A - \mu_B$ and the temperature T are the independent variables of the problem, while the "order parameter" m of the unmixing transition

$$m \equiv \Delta n/n, \quad n \equiv n_A + n_B, \quad \Delta n \equiv n_A - n_B \tag{3}$$

is directly recorded in the simulation: Here n_A denotes the number of A chains and n_B the number of B chains at a given instant of time. The Monte Carlo process thus includes two types of moves: local motions as shown in Figure 1 to relax the chain configurations and chain

relabeling trials (A → B or B → A, respectively), where one attempts to change the identity of a chain keeping its configuration fixed. Since the properties of species A and B are fully symmetric and in the critical region $\langle|m|\rangle_T$ is distinctly smaller than unity, there is only a very small correlation between the type of a chain (A or B) and its configurational properties (radius of gyration, etc.). Therefore, it is not necessary to fully relax the chain configuration from one chain relabeling trial to the next. In fact, near the critical point T_c, m is a very slowly relaxing variable, and because of this "critical slowing down"[72] it is necessary to have a very large number of relabeling trials per chain.[73] Thus we carry out one relabeling attempt per chain once after every canonical step per monomer, where motions of the type shown in Figure 1 are attempted.

As is standard in Monte Carlo sampling,[73] attempted moves are acceptable only if their transition probability $W(c\rightarrow c')$ exceeds a random number ζ uniformly distributed between zero and unity. This transition probability to go from the old configuration (c) to the new configuration (c') can be expressed in terms of the energies of these configurations (E, E') and their order parameters (m, m') as[41,65]

$$W(c\rightarrow c') = \min\left\{1, \exp\left[\frac{\Delta\mu(m'-m)Nn}{2k_BT}\right]\exp\left[-\frac{(E'-E)}{k_BT}\right]\right\} \quad (4)$$

Note that the symmetry ($N_A = N_B = N$) of our model implies that in the grand-canonical partition function of the polymer system the term $\exp[(\mu_A n_A N_A + \mu_B n_B N_B)/k_BT]$ can be rewritten as $\exp[N(\mu_A + \mu_B)n/(2k_BT)]\exp[N\Delta\mu mn/(2k_BT)]$. Since in each simulation run n is constant, the first exponential does not change and it is only the term $\exp[N\Delta\mu mn/(2k_BT)]$ which needs to be taken into account here. Equation 4 is constructed in order to satisfy a detailed balance with the grand-canonical distribution function, as usual.[65,73] For the canonic moves (shown in Figure 1) in addition to eq 4 (with $m = m'$, of course) self-avoiding and bond restrictions have to be obeyed while the latter two are automatically fulfilled in the grand-canonical relabeling steps because $N_A = N_B = N$. This is one place where the symmetry of the systems strongly reduces the simulational effort.

For a mixture with asymmetric chain lengths, taking out a chain also would not be a problem, but insertion of the longer type of chain would have a very low acceptance probability, as new bonds at one chain end need be compatible with excluded-volume and bond length constraints, which is very hard to satisfy in a dense system. Another advantage of symmetric mixtures is that the construction of phase diagrams is greatly facilitated by the fact that a change of label (A → B, B → A) leaves the problem invariant, if we also reverse the sign of $\Delta\mu$. This implies that phase coexistence occurs for $\Delta\mu = 0$ and that the phase diagram of the system is symmetric around the critical volume fraction ϕ_c corresponding to $m = 0$:

$$\phi_c = \phi_{A_c} = \phi_{B_c} = \phi/2, \quad \phi_A = \phi_c(1+m), \quad \phi_B = \phi_c(1-m) \quad (5)$$

In principle, what the Monte Carlo simulation[73] yields is a number $\mathcal{N}$ of configurations which are distributed proportional to the distribution

$$P_{T,\Delta\mu}(E,m) = \frac{1}{Z(T,\Delta\mu)}\exp\left[\frac{\Delta\mu mNn}{2k_BT}\right]\exp\left(-\frac{E}{k_B/T}\right)\Gamma(E,m) \quad (6)$$

where $Z(T,\Delta\mu)$ is the grand-canonical partition function,

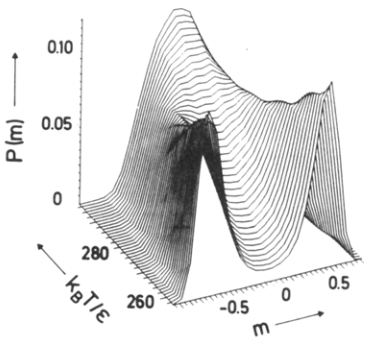

Figure 2. Distribution function $P(m)$ of the order parameter m plotted over a range of temperatures for $N = 128$ and $L = 80$. Such distributions have been extrapolated with the help of eqs 8 and 9 from runs at the single temperature $k_bT/\epsilon = 266.4$. The number of (statistically independent) configuration samples was $N = 16.800$.

and we assume that the only variables relevant for the phase transition of the system are E and m; i.e., all other configurational variables are "integrated out". Then $\Gamma(E,m)$ is the number of states in the phase space that have energy E and order parameter m. What is measured in the simulation is now a histogram $H(E,M)$ of these variables E and m, which for a large number N of statistically independent measurements approximates $P_{T,\Delta\mu}(E,m)$, apart from statistical errors:

$$\mathcal{N}^{-1}H_{T,\Delta\mu}(E,m) \approx P_{T,\Delta\mu}(E,m) \quad (7)$$

The idea of the histogram method[61,65,74] is that $H_{T,\Delta\mu}(E,m)$ can be used to estimate $P_{T',\Delta\mu'}(E,m)$ at a whole range of neighboring values $T',\Delta\mu'$ around $T,\Delta\mu$, since eqs 6 and 7 imply

$$P_{T',\Delta\mu'}(E,m) \approx \frac{Z(T,\Delta\mu)}{Z(T',\Delta\mu')}\exp\left[\frac{\Delta\mu' mNn}{2k_BT'} - \frac{\Delta\mu mNn}{2k_BT}\right]\exp\left(\frac{E}{k_BT} - \frac{E}{k_BT'}\right)\frac{H_{T,\Delta\mu}(E,m)}{\mathcal{N}} \quad (8)$$

Of course, this method is practically useful only[61,65] for such a range of parameters where the exponential functions do not emphasize values of E,m far out in the wings of the measured histogram H. In our case, where the number of chains in the simulated systems is never extremely large, all distributions are rather broad and this reweighting technique works over a reasonably broad range of temperatures and fields. As an example, Figure 2 shows distributions $P_T(m)$ defined as

$$P_T(m) \equiv \int P_{T,\Delta\mu=0}(E,m)\,dE \quad (9)$$

which were obtained from such extrapolations using a simulation at a single state point ($T,\Delta\mu=0$). For more details on this technique, for instance, how to handle the ratio of partition functions in eq 8, see ref 65, where also the extension to combine information from several state points ($T,\Delta\mu$) is described. From Figure 2 we can easily recognize that the distribution function is peaked at $m = 0$ at high temperatures ($T > T_c$), while approaching T_c the distribution broadens and splits up into two peaks, representing the two coexisting phases for $T < T_c$: the peak with $m > 0$ represents the A-rich branch of the coexistence curve and the peak with $m < 0$ the B-rich branch (cf. eq 5). Of course, there is some systematic dependence of these distributions on the finite linear dimension L of the simulation box.[41,42,65,73] This dependence is utilized by applying a finite-size scaling analysis,[62-65] which is briefly described next. As explained

below, in terms of the variables n, $t \equiv T/T_c - 1$, and $\mu \equiv N\Delta\mu/k_BT_c$ the distribution function $P(m)$ is written as a product of a scale factor $n^{\beta/d\nu}$ and a scaling function $\tilde{P}$:

$$P(m) = C_3 n^{\beta/d\nu} \tilde{P}(C_1 n^{1/d\nu} t, C_2 n^{\beta\delta/d\nu} \mu, C_3 n^{\beta/d\nu} m, N|t|^{(4-d)/(d-2)}) \quad (10)$$

Here β, δ, and ν are critical exponents that are defined below, d is the dimensionality of the system ($d = 3$ here), and C_1, C_2, and C_3 are "nonuniversal"[62] scale factors while the function $\tilde{P}(z_1,z_2,z_3,z_4 \to 0)$ is known to be "universal".[62] As is well-known from the theory of critical phenomena[44,62,63,75] certain quantities (e.g., the critical exponents) do not depend on the details of a physical system (or a model system) but are the same for a whole class of systems, and this is meant by "universality". The critical exponents β, δ of the order parameter, and ν of the correlation length ξ of order parameter fluctuations are defined as follows:[44]

$$\lim_{n\to\infty} \langle |m| \rangle_{T,\mu=0} = \lim_{\mu\to 0} \lim_{n\to\infty} \langle m \rangle_T = \hat{B}(-t)^\beta, \quad |t| \to 0 \quad (11)$$

$$\lim_{n\to\infty} \langle m \rangle_{T=T_c} = \hat{D}\mu^{1/\delta}, \quad t = 0 \quad (12)$$

and

$$\xi = \hat{\xi}^{\pm}|t|^{-\nu}, \quad |t| \to 0, \quad \mu = 0 \quad (13)$$

In eqs 11 and 12 $\hat{B}$ and $\hat{D}$ are the (nonuniversal) "critical amplitudes"[44] of the order parameter, while $\hat{\xi}^{\pm}$ are the critical amplitudes of the correlation length (the two signs $\pm$ refer to the sign of t above or below T_c, respectively). In eq 11, we have expressed the fact that an (infinitesimal) "field" $\mu \neq 0$ is necessary to break the symmetry between the two ordered states of the system for $T < T_c$ (alternatively one can consider $\langle |m| \rangle_T$ instead of $\langle m \rangle_T$). Note also that these power laws are only asymptotically valid in the specified limits ($|t| \to 0$ or $\mu \to 0$, respectively): similarly, it is understood that these limits are also taken in eq 10, together with the limits $N \to \infty$ and $n \to \infty$ taken such that the arguments z_1, z_2, z_3, and z_4 of the scaling function remain finite.

Before we explain the motivation for the finite-size scaling from eq 10 we mention that another critical exponent γ and associated amplitudes $\hat{C}^{\pm}$ need to be defined for the "order parameter susceptibility"[44] χ_m, which is related to the collective scattering intensity at zero wavevector $\vec{k} \to 0$

$$k_BT\chi_m \equiv L^d(\langle m^2 \rangle_T - \langle m \rangle_T^2) = \{L^d/[2^d nN(1-\phi_v)]\} S_{coll}(\vec{k}\to 0) = \frac{S_{coll}(k\to 0)}{(1-\phi_v)^2} \quad (14)$$

$$k_BT\chi_m(\mu=0) = \hat{C}^{\pm}|t|^{-\gamma}, \quad |t| \to 0 \quad (15)$$

We now comment on eq 10. The factor $c_3 n^{\beta/d\nu}$ in front of the scaling function simply is necessary to ensure proper normalization, $\int dm\, P(m) = 1$, which must hold irrespective of the values of the variables μ, t, and N.

We now discuss the physical meaning of the above arguments z_1, z_2, z_3, and z_4 that appear in the scaling function $\tilde{P}$ (eq 10). First we note that in our model the number of chains n is related to the linear dimension L of the simulated boxes by $n = \phi L^d/(2^d N)$, where 2^d is the monomer volume of the bond fluctuation model in d dimensions. Thus the argument $z_1 = c_1 n^{1/d\nu} t \propto L^{1/\nu} \propto (L/\xi)^{1/\nu}$ (cf. eq 13) and thus expresses the basic principle of finite-size scaling[62-65] that the characteristic lengths should be compared ("L scales with ξ"). In fact, a more traditional scaling ansatz appearing often in the literature is (disregarding the last argument z_4 since we now consider a fixed finite N and then $z_4 \to 0$ holds in the asymptotic critical region)[62-65]

$$P(m) = L^{\beta/\nu} \tilde{P}'(L^{1/\nu} t, L^{\beta\delta/\nu} \mu, L^{\beta/\nu} m) \quad (16)$$

where $\tilde{P}'$ results from $\tilde{P}$ by absorbing the various constants that come in when we transform from $n^{1/d}$ to L. While eq 16 is perfectly valid when we consider a fixed N, one has to be more careful when one wishes to study the effects of varying N, of course, since N enters the above transformation between n and L^d. While in an Ising spin system where L is measured in units of the lattice spacing the number of spin degrees of freedom always simply is equal to L^d, the number of degrees of freedom n of A $\leftrightarrow$ B interchanges (which in a sense corresponds to the flipping of an Ising spin!) changes when we change N at fixed L, and it really is the smallness in the number of these degrees of freedom that is responsible for the "finite-size effects" and thus it is n which should be used as the basic variable. Therefore, eq 10 is more useful than eq 16, because any conclusion drawn from eq 16 holds only for N being strictly fixed, while eq 10 will allow us to consider variations of N as well.

The general principle underlying eq 10 is that $P(m)$ does not depend on the five variables n, t, μ, m, and N in the most general form, but rather one has a function of only four variables z_1, z_2, z_3, and z_4, which result from incorporating the n dependence by suitable power laws. While the power law relating t and z_1 has already been motivated above, the powers of n appearing in z_2 and z_3 are a simple consequence of the fact that eq 10 must be consistent with eqs 11 and 12 in the appropriate limits. One can see this by taking appropriate moments of the distribution function $P(m)$, k being an integer

$$\langle m^k \rangle \equiv \int dm\, m^k P(m) = c_3^{-k} n^{-k\beta/d\nu} \tilde{f}_k(c_1 n^{1/d\nu} t, c_2 n^{\beta\delta/d\nu} \mu, Nt^{(4-d)/(d-2)}) \quad (17)$$

where $\tilde{f}_k(z_1,z_2,z_4)$ is another scaling function. Consider first the limits $\mu \to 0$ and $n \to \infty$ (cf. eq 11, for $k = 1$ in eq 17): this limit can yield the result of eq 11 only if $\tilde{f}_1(z\to\infty,z_2,z_4) \sim (-z_1)^\beta$, and we see that then the prefactor $n^{-\beta/d\nu}$ is indeed canceled. Thus the power law $n^{\beta/d\nu}$ that was used as the scaling power of m in eq 10 was indispensable for having the power law eq 11. Similarly, eq 12 can result only if $\tilde{f}_1(0,z_{2\to\infty},0) \sim z_2^{1/\delta}$, and indeed again the prefactor $n^{-\beta/d\nu}$ in eq 17 for $k = 1$ is canceled. Thus the power law $n^{\beta\delta/d\nu}$ relating z_2 to μ in eq 10 was indispensable for consistency with eq 12.

At this point we note that $P(m)$ for $\mu = 0$ is manifestly symmetric (Figure 2), as it must be due to the symmetry of our model against A $\leftrightarrow$ B interchanges; thus odd moments vanish for $\mu = 0$. It then makes sense to consider also moments of corresponding nonnegative quantities

$$\langle |m|^k \rangle = c_3^{-k} n^{-k\beta/d\nu} \tilde{f}_k'(c_1 n^{1/d\nu} t, c_2 n^{\beta\delta/d\nu} \mu, Nt^{(4-d)/(d-2)}) \quad (18)$$

Here $\tilde{f}_k'$ again is a scaling function which is identical to $\tilde{f}_k$ for k = even but differs from $\tilde{f}_k$ for k = odd and z_2 being small. Equation 18 is convenient for the estimation of both the order parameter (eq 11) and zero-field susceptibility below T_c:

$$k_BT\chi_m = L^d(\langle m^2 \rangle_{T,\mu=0} - \langle |m| \rangle_{T,\mu=0}^2), \quad T < T_c \quad (19)$$

while for $T > T_c$ eq 14 must be used.[65,73]

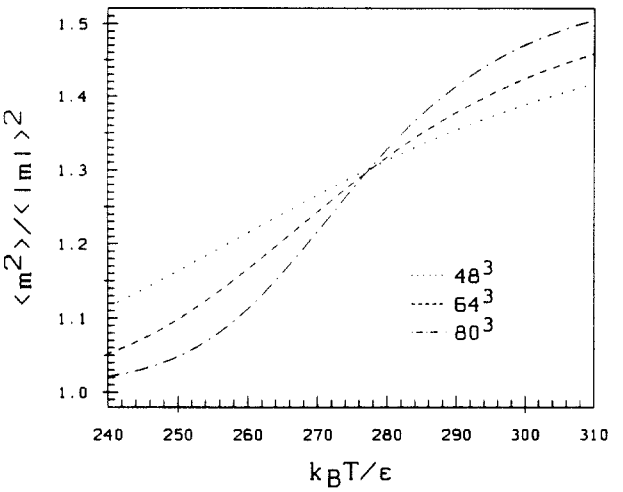

Figure 3. Reduced moment ratio $U_{12}^{21} = \langle m^2 \rangle_T / \langle |m| \rangle_T^2$ plotted vs k_BT/ϵ for $N = 128$. Different curves indicate data for different linear dimensions, as shown in the plot.

The last argument $z_4 = Nt^{(4-d)/(d-2)}$ in eqs 10, 17, and 18 is included in order to describe the crossover from Ising-like critical behavior,[44,62,75] in $d = 3$

$$\beta \approx 0.324, \quad \gamma \approx 1.239, \quad \nu \approx 0.629, \quad \delta \approx 4.82 \qquad (20)$$

to mean-field (Landau-theory-like) critical behavior[44]

$$\beta^{MF} = \frac{1}{2}, \quad \gamma^{MF} = 1, \quad \nu^{MF} = \frac{1}{2}, \quad \delta^{MF} = 3 \qquad (21)$$

According to the Ginzburg[76] criterion adopted for polymers, eq 21 describes the critical behavior (eqs 11–13 and 15) if $|t|$ is small but N so large that[32]

$$z_4 = N|t|^{(4-d)/(d-2)} \gg z_4^{cross} \qquad (22)$$

while close enough to T_c, i.e., for $z_4 \ll z_4^{cross}$, the universality principle[77] also implies Ising-like critical behavior for polymer mixtures (in $d = 3$). For z_4, near z_4^{cross} a smooth crossover from one type of critical behavior to the other should occur. The Ginzburg variable in the direction of the critical isotherm ($T = T_c$, $\mu \neq 0$), which is $N^{3/2}\mu$ in $d = 3$, does not need to be considered explicitly since it is a function of the other three variables in eqs 17 and 18; i.e., there is no new variable.[65]

If only a fixed N is considered that is not too large, so that at the temperatures of interest $z_4 \ll z_4^{cross}$ is valid, the argument $z_4 = N|t|^{(4-d)/(d-2)}$ in eqs 10, 17, and 18 can be omitted. Then any chain-length dependence in eqs 10, 17, and 18 can arise only via the scale factors c_1, c_2, and c_3.

From eqs 17 and 18 we recognize that for $\mu = 0$ and fixed N one can form combinations of moments that depend on a single scaling variable $z_1 = c_1 n^{1/d\nu} t \sim L^{1/\nu} t$ only and do not exhibit an extra power of n (or of L, respectively) in the prefactor, if the product of powers (kl) in the numerator equals the product of powers in the denominator (ij)

$$U_{ij}^{lk} \equiv \langle |m|^k \rangle_T^l / \langle |m|^i \rangle_T^j = [\tilde{f}_k'(c_1 n^{1/d\nu} t, 0)]^l / [\tilde{f}_i(c_1 n^{1/d\nu} t, 0)]^j \qquad (23)$$

Here the crossover scaling argument z_4 has been omitted since N is kept fixed for this consideration.

Combinations of moments of the type shown in eq 23 are useful since for $t = 0$ the n dependence (or L dependence, respectively) completely drops out. Consequently,[65] plotting such a ratio versus temperature for several values of L, one should obtain a family of curves intersecting in a unique point (Figure 3), the abscissa of that point being the critical temperature T_c. The same argument also holds in the mean-field regime for large (fixed) N. Only the exponents of n differ, which is irrelevant at $t = 0$. This technique frequently has been used for the reduced fourth-order cumulant[41,62] U_{22}^{41}. Since low-order moments are more accurately estimated than high-order ones, we here use the quantity U_{12}^{21} (Figure 3). It is seen that these intersection points already yield fairly accurate estimates of T_c. The results for T_c will be discussed further in the next section.

3. Monte Carlo Results for Phase Diagrams, Spinodals, and Effective Flory–Huggins Parameters

As discussed in section 2, phase coexistence between A-rich and B-rich phases occurs in our symmetrical model for $\mu = 0$ and $T < T_c$, and the coexistence curve between the two phases is symmetric around the critical volume fraction $\phi_c = \phi/2$ (cf. eq 5)

$$\phi_A^{coex} = \frac{1}{2}\phi(1 + \langle m \rangle_{spont}), \quad \phi_B^{coex} = \frac{1}{2}\phi(1 - \langle m \rangle_{spont}) \qquad (24)$$

where $\langle m \rangle_{spont}$ is the "spontaneous order parameter" that appears in the thermodynamic limit $n \to \infty$ ("spontaneously broken symmetry"[44,65]). Of course, for finite systems there is no strict breaking of symmetry: as can be seen from the probability distribution $P(m)$ shown in Figure 2, there always is a nonzero probability for a system (that has $\mu = 0$ so both peaks for $T < T_c$ in Figure 2 are indeed equally high) to pass from one peak through the minimum to the other peak. Thus, as mentioned already in eq 11, we have to "put in" the broken symmetry by taking the absolute value $\langle |m| \rangle_{T,\mu=0}$ instead of $\langle m \rangle_{T,\mu=0}$ since the latter would be zero for any finite L. Of course, also $\langle |m| \rangle_{T,\mu=0}$ does depend on L or n, respectively (near T_c this is described by eq 18), but one expects that as $L \to \infty$ one will have a smooth approach of $\langle |m| \rangle_{T,\mu=0}$ toward $\langle m \rangle_{spont}$, the quantity needed to characterize the coexistence curve. This expectation not only is contained in the theory of finite-size scaling[62–64] but also is confirmed by practical experience with various models[41,42,73] and once more by the present data (Figure 4). Since the system is symmetric with respect to the sign of $\langle m \rangle_{spont}$ it suffices to consider $\langle m \rangle_{spont} > 0$, and hence only the region with a positive order parameter is displayed in Figure 4. In terms of volume fractions, we thus display the region from $\phi_A = \phi_c = \phi/2$ ($\langle |m| \rangle = 0$) to $\phi_A = \phi$ ($\langle |m| \rangle = 1$); the region from $\phi_A = 0$ to $\phi_A = \phi_c$ is simply obtained from a mirror image at the abscissa. For clarity, only the immediate neighborhood of the critical temperature for every choice of N is shown. It is seen that for temperatures more than 10% below T_c, all data for different L superimpose on a unique curve; i.e., finite-size effects then are negligible. Nearer to T_c, however, the curves for different choice of L are distinct, and $\langle |m| \rangle$ in fact stays nonzero above T_c as well. This kind of finite-size effect, of course, is well-known[41,42,64,73] and expected from theory,[62–65] and it does not prevent us from carrying through a quantitatively reliable extrapolation to the thermodynamic limit, $L \to \infty$. In fact, eq 18 suggests to plot $\langle |m| \rangle L^{-\beta/\nu}$ vs $L^{1/\nu} t$ since for $\mu = 0$ and small Nt we have for fixed chain length

$$\langle |m| \rangle = C_3^{-1} n^{-\beta/d\nu} \tilde{f}_1'(c_1 n^{1/d\nu} t, 0) \Rightarrow$$
$$\langle |m| \rangle L^{\beta/\nu} \equiv \tilde{f}_1'(\text{const } L^{1/\nu} t, 0) \qquad (25)$$

i.e., for each fixed N curves for different values of L should coincide on a single "master curve", representing the scaling function. For large and negative values of the argument $z_1 = c_1 n^{1/d\nu} t$ where $\langle |m| \rangle$ is independent of L or n, we expect a behavior, as already mentioned in the previous section

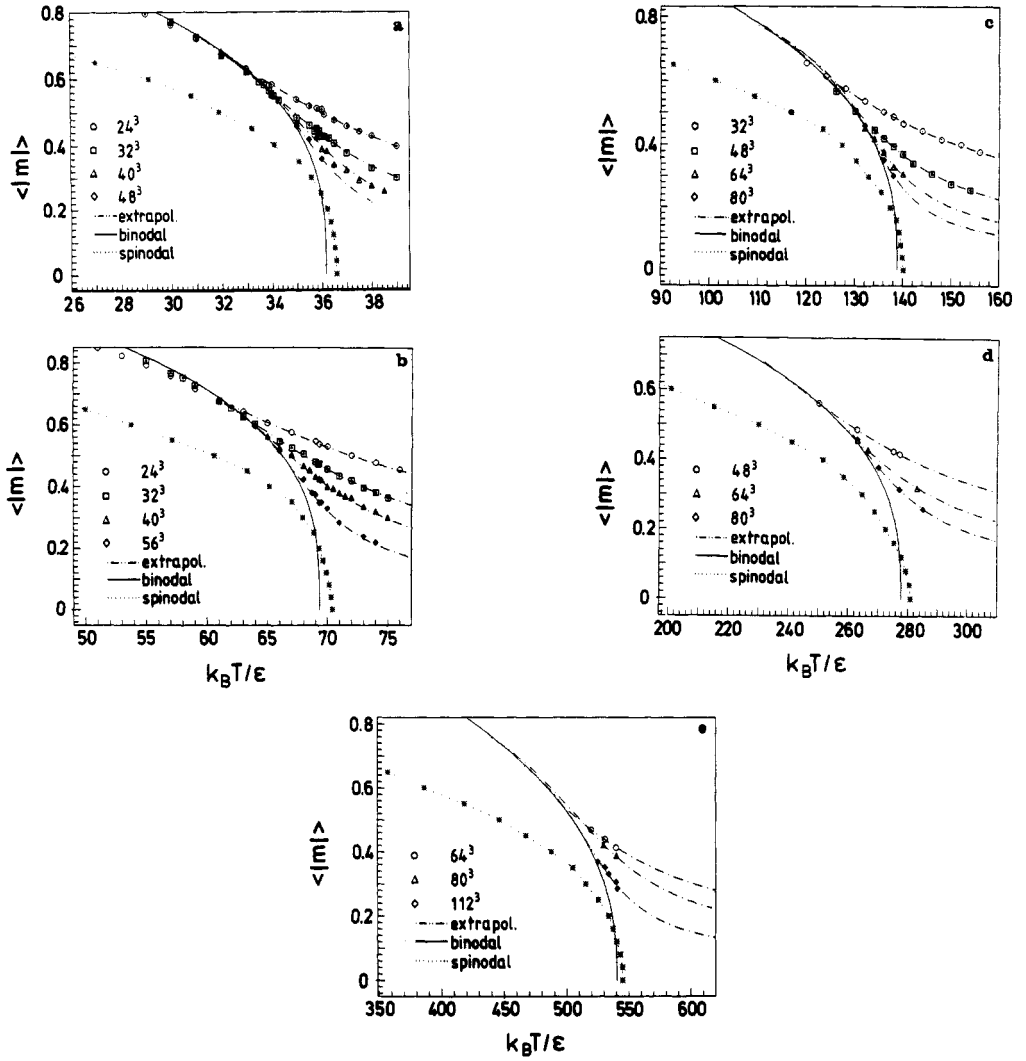

Figure 4. Order parameter $\langle|m|\rangle$ plotted vs temperature k_BT/ϵ for $N = 16$ (a), $N = 32$ (b), $N = 64$ (c), $N = 128$ (d), and $N = 256$ (e). Points characterized by lattice sizes were directly recorded in the simulations, while the dash-dotted curves connecting them are not "guides to the eye" (as in ref 42, for instance) but were constructed from the corresponding probability distribution (such as shown in Figure 2a,b) via the multiple histogram method.[65] Having established the accuracy of this method with many directly recorded control data for $N = 16$ and $N = 32$, only few such control data are generated for $N = 128$ and $N = 256$, for the sake of economical use of computer time. Full curves are the estimates for the coexistence curves that result for $L \to \infty$ from the finite-size scaling analysis (see Figure 18). Dotted curves, however, are guides to the eye only through the stars obtained as estimates for the effective spinodal curve, as explained below.

$$\tilde{f}_1'(z_1 \to -\infty, 0, 0) = \hat{B}(-z_1)^{\beta} \tag{26}$$

where $\hat{B}$ is a universal constant because $\tilde{f}_1'$ is a universal function of its arguments. Equation 26 is the only possibility for having no dependence on L in eq 17 and to extract the power law (eq 11) from the finite-size scaling behavior (eq 25). Figure 5 shows that this analysis proves to be a good working tool to represent the data. Unlike the previous work by Sariban and Binder[41,42] where critical exponents as quoted in eq 20 were *assumed* to hold for polymer mixtures as well and thus were simply used as an *input* in eq 25, we here prefer to extract the exponents from the data analysis itself, to avoid any bias that might result from the crossover between mean-field (eq 21) and Ising behavior (eq 20), that is expected for very long chains. We defer a discussion of this analysis of critical exponents to the next section. Of course, the power law (eqs 11 and 26) deduced from the data from the finite-size scaling analysis as in Figure 5 is supposed to hold for $|t| \to 0$ only; farther below T_c systematic deviations from this power law are expected. We can see these systematic deviations very distinctly in Figure 4b, for instance, at $k_BT/\epsilon = 60$ and below. The fact that there the power law overestimates the order parameter is related to the rather large value of the amplitude $\hat{B} = 1.365$; if eq 11 would hold for $T \to 0$, the order parameter would exceed unity, while our normalization unity is its maximum value.

We next turn to discuss the "extrapolated spinodal" curves included in Figure 4, warning the reader from the start that according to general principles of statistical mechanics "spinodal curves" are a somewhat ill-defined concept,[32,78,79] apart from mean-field-like limiting cases. For a system with Ising-like critical behavior a spinodal is defined only as a result of a particular extrapolation procedure.[80] The extrapolation procedure used here is precisely the same as commonly applied experimentally: This is motivated by the fact that Flory–Huggins theory[6,9] would predict a vanishing of the inverse collective scattering intensity $S_{coll}(\vec{k} \to 0)$ at the spinodal

$$[S_{coll}(\vec{k} \to 0)]^{-1} = \frac{1}{4N}\frac{\phi}{\phi_A\phi_B} - \frac{1}{2}\chi(T) \tag{27}$$

i.e., a spinodal curve is obtained then by the equation (using also eq 5)

$$\chi_{sp}(T) = \phi/[2N\phi_A\phi_B] = 2/[\phi N(1 - m^2)] \tag{28}$$

Now in the Flory–Huggins theory the temperature de-

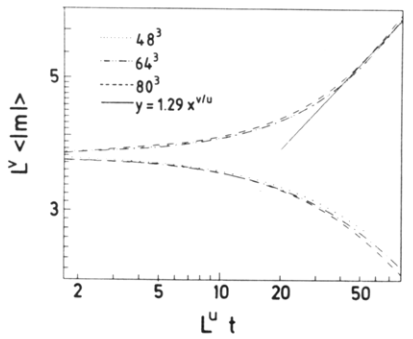

Figure 5. Finite-size scaling plot of the order parameter $\langle|m|\rangle$ for $N = 128$, using $k_BT_c/\epsilon = 277.7$, and measured effective exponents. Note that the lower set of curves represents $T > T_c$ ($t > 0$) and the upper set of curves $T < T_c$ ($t < 0$). The straight line describes the equation $\tilde{f}_1' = 1.29\ (-z_1)^{\beta}$. Different curves represent three choices of $L = 48$ (dotted), $L = 64$ (dashed-dotted), and $L = 80$ (full) and are the functions extracted from the histograms. The residual small systematic deviations between these curves may reflect both the statistical error of the histograms and corrections to finite-size scaling.

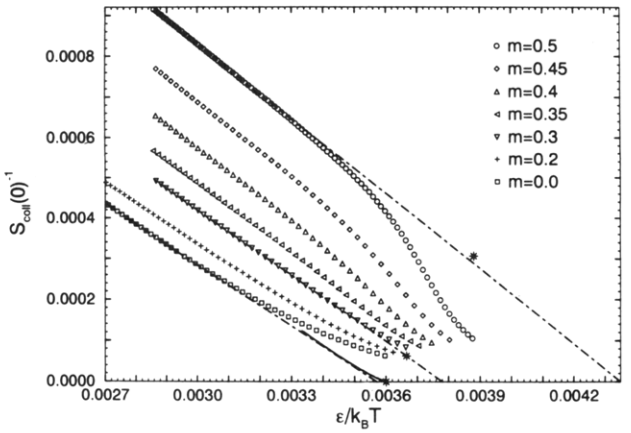

Figure 6. Plot of $1/S_{coll}(\vec{k}\to 0)$ vs ϵ/k_BT for $N = 128$ and $L = 80$ and several choices of $\langle m\rangle$ as indicated in the figure. For $m = 0$, 0.3, and 0.5 the straight lines yielding $T_{sp}(m)$ and the corresponding stars denoting the corresponding points in the thermodynamic limit where $\Delta\mu = 0$ are also shown. The solid line is the thermodynamic limit for $m = 0$.

pendence of $\chi(T)$ should be linear in $1/T$ and nonsingular at $T = T_{sp}(m)$. Therefore, eq 28 can be inverted to yield T_{sp} as a function of m. In fact, from the Flory lattice model one would conclude, in our notation

$$\chi(T) = 2z\epsilon/k_BT \tag{29}$$

z being the effective coordination number, but in practical experimental work one rather has to use a more general expression[8] with phenomenological concentration-dependent coefficients $a(m)$ and $b(m)$

$$\chi_{exp}(T) = a(m)/T + b(m) \tag{30}$$

However, in any case one expects that near $T = T_{sp}(m)$ one may use a linear variation of $\chi(T)$ in $1/T$, and this suggests to try a plot of $[S_{coll}(\vec{k}\to 0)]^{-1}$ as a function of ϵ/k_BT (Figure 6): If a linear region in this plot can be identified, one can obtain the intercept with the abscissa of the straight line that is fitted to the linear region, and this intercept defines the temperature of the spinodal, $T_{sp}(m)$. It is obvious from Figure 6 that in the critical region the actual data in the plot of $[S_{coll}(\vec{k}\to 0)]^{-1}$ vs ϵ/k_BT deviate from linearity, even for rather large chains as used here ($N = 128$). In the region where finite-size effects are not yet pronounced, this curvature is due to the nonclassical critical exponent $\gamma > 1$ ($\gamma \approx 1.24$; cf. eq 20) in the power

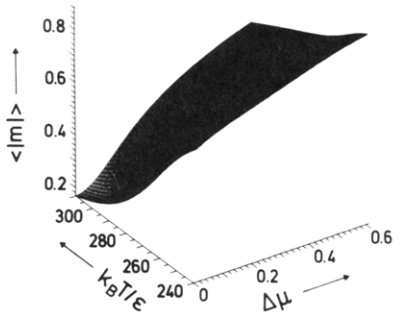

Figure 7. Plot of $\langle|m|\rangle$ as a function of T and $\Delta\mu$ for $N = 128$ and $L = 80$ in the critical region.

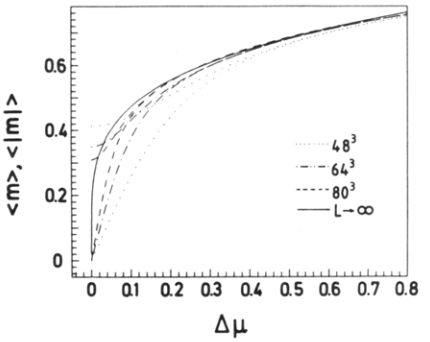

Figure 8. Plot of $\langle|m|\rangle$ (dotted curves) and $\langle m\rangle$ (dash-dotted curves) versus $\Delta\mu$, for $N = 128$, $T = T_c = 277.7k_B/\epsilon$, and three choices of L as indicated. The solid curve shows the extrapolation obtained in the thermodynamic limit $L \to \infty$.

law (eq 15). In fact, a linear behavior would be implied by mean-field theory ($\gamma^{MF} = 1$; cf. eq 21). Although this singular behavior of eq 15 applies for $\mu = 0$ (and hence $\langle m\rangle \neq 0$) only, it also affects the behavior for $\mu \neq 0$ (and hence $\langle m\rangle \neq 0$) via the scaled equation of state.[44,62,80] Similar curvature as in Figure 6 has also been seen in previous simulations on much shorter chains[42,43] and in various experiments.[67-70] This curvature is ignored in the linear extrapolation in Figure 6, and thus it happens (Figure 4) that the extrapolated spinodal near the critical point $\{T_{sp}(m=0)\}$ lies slightly above the coexistence curve, which makes no physical sense, of course: in mean-field theory, where a spinodal curve makes perfect sense,[32,78,79] it lies always below the coexistence curve and touches the latter in the critical point only. But our data are consistent with recent experimental findings[68] where it was found that the "mean-field T_c" $\{=T_{sp}(m=0)\}$ exceeds the true T_c. From Figure 4 it is suspected that the relative distance of the extrapolated spinodal $T_{sp}(0)$ for $\langle m\rangle = 0$ from the critical temperature T_c decreases with increasing chain length. Unfortunately, the smallness of $[T_{sp}(m=0) - T_c]/T_c$ prevents a quantitative analysis. In the limit $N \to \infty$ this difference whould vanish completely because of the Ginzburg criterion since the systems should then belong to the mean-field universality class with the exponent $\gamma = 1$ and therefore there should be no more curvature in the line for $m = 0$, $L \to \infty$ in Figure 6.

At this point, we comment how $S_{coll}(\vec{k}\to 0)$ is obtained for fixed $\langle m\rangle$ from a grand-canonical simulation where the thermodynamically conjugate variable $\Delta\mu$ rather than $\langle m\rangle$ is held fixed. A crucial point of this analysis is clearly the fact that the reweighting technique[65] (eq 8) allows us to extract the full equation of state $\langle m\rangle = f(T,\Delta\mu)$ from the recorded histograms $H(E,m)$ over a wide range of T and $\Delta\mu$ in the critical region (Figure 7). Of course, there the size effects need to be carefully considered (Figure 8), but again finite-size scaling methods allow a reliable extrapolation $L \to \infty$. From the histograms $H(E,m)$ the

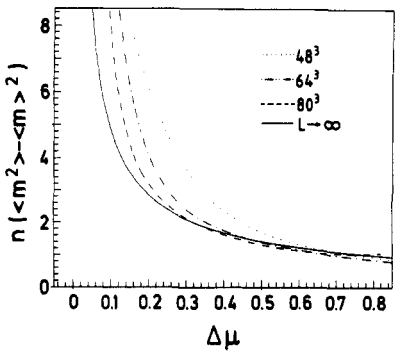

Figure 9. Normalized order parameter fluctuation $n[\langle m^2\rangle - \langle m\rangle^2]$ plotted vs $\Delta\mu$ for $N = 128$, $T = T_c$, and three different system sizes. The solid curve denotes the extrapolated result for the thermodynamic limit.

reweighting technique allows an estimation of $S_{coll}(\vec{k}\to 0)$ as function of μ as well (Figure 9) using fluctuation relations (eq 14). Combining the information from Figures 8 and 9, we can clearly obtain $S_{coll}(\vec{k}\to 0)$ as a function of $\langle m\rangle$ for $T = T_c$. This procedure can also be done at other temperatures but is somewhat cumbersome to apply, since the finite-size scaling analysis is rather involved if both μ and t are nonzero. Since the region where $[S_{coll}(\vec{k}\to 0)]^{-1}$ is approximately linear is rather far away from the transition points, finite-size effects are quite small[65] in this region, and we therefore used the largest system size to generate Figure 6. The upward bending of $1/S(0)$ for large $S(0)$ and small m has two reasons: the exponent $\gamma > 1$ and finite-size effects. To disentangle these two effects, the solid line shows $1/S(0)$ for $m = 0$ in the limit $L \to \infty$ obtained from finite-size scaling. This line ends in the critical point and demonstrates clearly that $\gamma > 1$ is responsible for $T_{sp}(0) > T_c$. It also shows that most of the upward bending of the *measured* curve is due to finite-size effects.

For $m > 0$ we have to adjust the chemical potential $\Delta\mu$ to keep m fixed when the temperature is varied. In this case we still have one point of the $L \to \infty$ limit for each m following from the binodal in Figure 4d and the corresponding plot for the susceptibility in ref 65. From these points (shown as asterisks in Figure 6) we deduce that plotting $1/S(0)$ vs $1/T$ for fixed $m > 0$ in the thermodynamic limit will show straight lines even near the transition points, while the upward curvature for small m in Figure 6 is due to finite-size effects near the second-order critical point and the downward bending for large m stems from finite-size effects near *first-order* transition points ($\Delta\mu \approx 0$, $T < T_c$). Scaling at these first-order transitions is qualitatively different from that at second-order transitions and will be discussed in a future publication on asymmetric mixtures.

Data such as those displayed in Figure 9 can be immediately used to construct an effective Flory–Huggins χ parameter χ_{eff}, using eqs 5 and 27

$$(1-\phi_v)\chi_{eff}(T) = \frac{1}{2N}\frac{\phi^2}{\phi_A\phi_B} - 2\phi S_{coll}(\vec{k}\to 0)^{-1} = \frac{2}{N}(1-\langle m\rangle^2)^{-1} - 2\phi S_{coll}(\vec{k}\to 0)^{-1} \quad (31)$$

As is well-known, this is exactly equivalent to the experimental estimation of a χ parameter from scattering data.[31] Of course, the strong finite-size effect seen in the data for $S_{coll}(\vec{k}\to 0)$ as a function of $\Delta\mu$ (Figure 9) or of $\langle|m|\rangle$ as a function of $\Delta\mu$ shows up in a similar size effect in the data for $\chi_{eff}(T)$ vs ϕ_A plots (recall eq 5!) that are studied experimentally. As Figure 10b shows, converting the χ_{eff}-

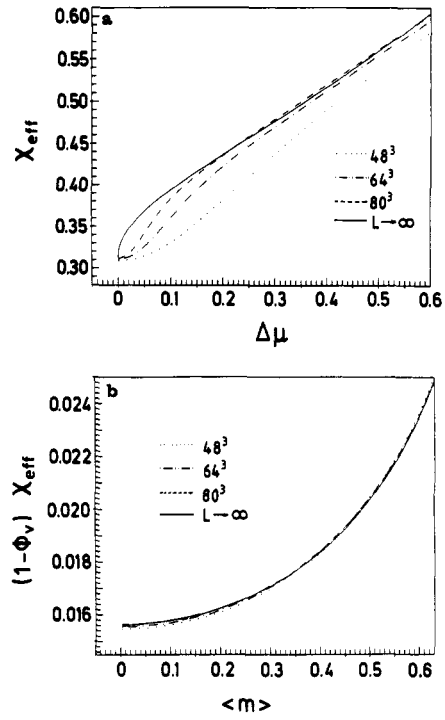

Figure 10. (a) Effective Flory–Huggins parameter χ_{eff} plotted vs $\Delta\mu$ for $N = 128$, $T = T_c$, and three different sizes. Here χ_{eff} is extracted from the data of Figure 9 with the help of eq 31. (b) χ_{eff} plotted vs the order parameter $\langle m\rangle$, converting the data from Figure 9 with the help of the relation $\langle m\rangle$ vs $\Delta\mu$ plotted in Figure 8b.

(T) vs $\Delta\mu$ plot with the help of the $\langle m\rangle$ vs $\Delta\mu$ plot (figure 8) to a $\chi_{eff}(T_c)$ vs $\langle m\rangle$ plot, the finite-size effects visible in both Figure 8 and Figure 10a have canceled to a large extent. Figure 10b thus implies a U-shaped concentration dependence of $\chi(T_c,\phi_A)$, with a minimum for $\phi_A = \phi_c$, and a strong increase both in the A-rich part of the blend ($\langle m\rangle \to 1$) and in the B-rich part of the blend ($\langle m\rangle \to -1$), since our model is exactly symmetric around $\langle m\rangle = 0$.

Of course, an effective χ parameter $\chi_{eff}(T)$ defined from eq 31 is not in any simple way related to microscopic interaction parameters (such as ϵ in our model); as already pointed out in the earlier work of Sariban and Binder,[41-43] the concentration and temperature dependence of $\chi_{eff}(T)$ is rather a spurious artifact of fitting a mean-field expression (such as eq 31) to data that reflect important deviations from mean-field theory due to various correlation effects. The temperature dependence of $\chi_{eff}(T)$ therefore is also by no means of the simple form given by eq 30, if data very close to T_c are analyzed. There the non-mean-field critical singularities (eqs 11–13, 15, and 20) show up in $\chi_{eff}(T)$, since this quantity essentially is a (normalized) second derivative of the free energy with respect to concentration ϕ_A. The singular behavior of free energy derivatives at T_c induces singularities in the temperature dependence of $\chi_{eff}(T)$. This becomes evident from our data, when we consider $\chi_{eff}(T)$ for $\mu = 0$, which means for $T < T_c$ that we follow a path along the coexistence curve. Figure 11 shows that along this path $\chi_{eff}(T)$ develops a cusp-shaped singularity at T_c. This behavior is understood by inserting eqs 11, 14, and 15 in eq 31. The inverse response function $[S_{coll}(\vec{k}\to 0)]^{-1}$ vanishes for a path along the coexistence curve as $[S_{coll}(\vec{k}\to 0)]^{-1} \propto (-t)^{\gamma}$, $\gamma \geq 1$, while the term $2[N(1-m^2)]^{-1} \propto 1 + \hat{B}^2(-t)^{2\beta}$ near T_c. Since very close to T_c Ising exponents are valid, i.e., $2\beta < 1$, this term yields for $t \to 0$ an infinite slope for $T < T_c$ but does not exist for $T > T_c$ and thus produces the cusp-shaped singularities in Figure 11. Also in the concentration dependence of χ_{eff}-

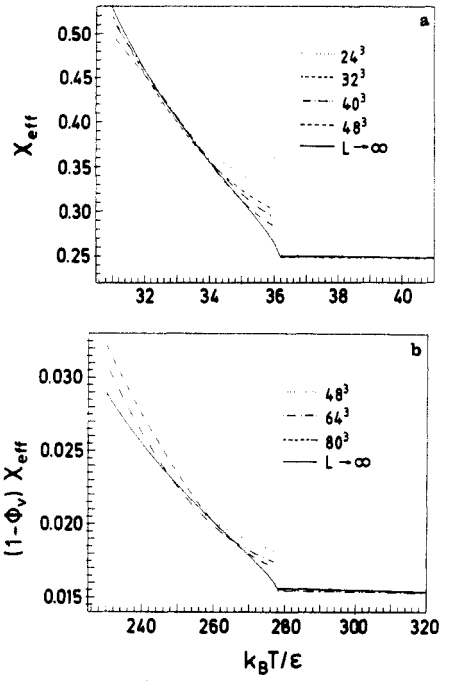

Figure 11. Effective Flory–Huggins parameter $\chi_{eff}(T,\mu=0)$ plotted vs k_BT/ϵ for $N = 16$ (a) and $N = 128$ (b). The broken curves indicate various finite lattice linear dimensions L, as indicated in the figure, while the solid curve is the extrapolated behavior for $L \to \infty$.

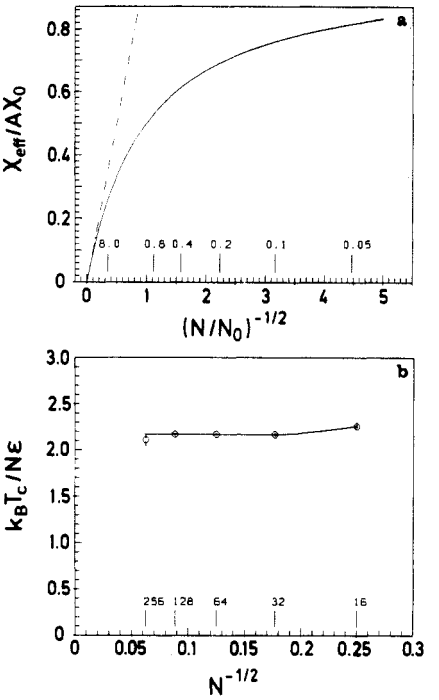

Figure 12. (a) Predicted variation of $\chi_{eff}/(A\chi_0)$ vs $(N_0/N)^{1/2}$ (eq 36). The broken straight line shows the asymptotic behavior $\chi_{eff}/(A\chi_0) \propto (N_0/N)^{1/2}$, while the marks indicate the scale for (N/N_0) itself. (b) Variation of the observed normalized critical temperature $k_BT_c/(\epsilon N)$ with $N^{1/2}$. Marks indicate the values of N chosen. Note that for large enough N the integral equation theory[50,51] predicts that this plot can be mapped on Figure 12a, by multiplying the coordinate scales with suitable constants, without any other adjustable parameters being available.

(T_c) there is a singular term, since eqs 10, 14, and 15 imply[44] near T_c

$$[S_{coll}(\vec{k}\to 0)]^{-1} = \hat{C}^{\pm}|t|^{\gamma}\tilde{S}_{coll}^{-1}(\mu|t|^{-\beta\delta}) \underset{T\to T_c}{\to} \text{const}\ \mu^{\gamma/\beta\delta} \quad (32)$$

where $\tilde{S}_{coll}^{-1}(\mu|t|^{-\beta\delta})$ is the scaling function of the structure factor. Once more, we have postulated that $\tilde{S}_{coll}^{-1}(z)$ for large z must be a power law, $\tilde{S}_{coll}^{-1}(z) \sim z^{\gamma/\beta\delta}$, such that the powers of $|t|$ cancel out. Combining eqs 12, 31, and 32, we conclude for $\chi_{eff}(T_c)$ that

$$\chi_{eff}(T_c) \propto \text{const}\ \langle m\rangle^{\delta-1} + \frac{2}{N}(1 + \langle m\rangle^2) \quad (33)$$

In the concentration dependence (Figure 10b) the first singular term is not easily seen, of course, since $\delta - 1 \approx 3.8 > 2$, and hence the regular term ($\propto \langle m\rangle^2$) resulting from eq 31 always dominates. Note that finite-size effects nearly cancel in Figure 10b. Also χ_{eff} is linear in N; i.e., plotting $N\chi_{eff}$ vs $\langle m\rangle$ would give the same master curve for all chain lengths.[66] Thus we believe that those concentration dependences of χ_{eff} are significant: they do not become smaller for increasing L or N, and there are therefore no artifacts resulting from finite-size effects.

A very strong renormalization of the interaction parameter (defined via eq 29) has in fact been predicted by the integral equation theory of Schweizer and Curro:[50,51] however, their theory does not lead to the correct Ising critical behavior (eq 20), which one should have also in polymer mixtures by the universality principle,[77] but rather their use of the "mean spherical approximation" implies that the critical exponents of the so-called "spherical model"[77,82] occur

$$\beta^s = {}^1/_2, \quad \gamma^s = 2, \quad \delta^s = 5, \quad \nu^s = 1 \quad (34)$$

Clearly, these numbers deviate from the Ising model results (eq 20) even more than those of the Flory–Huggins mean-field theory (eq 21), and thus the description of critical-point singularities in the framework of this integral equation theory should not be trusted, as recognized by the authors themselves.[50] The origin of the renormalization of the interaction strength in this theory[50] is a kind of screening effect within the correlation volume of a Gaussian coil.[83] The result is a reduction of the ratio of the effective χ parameter versus the Flory χ parameter such that[50,51,83]

$$\frac{\chi_{eff}(T)}{\chi_0(T)} = \frac{A}{1 + B[N^2/R_g^3]} \quad (35)$$

where $\chi_0(T)$ is the Flory χ parameter (given by eq 29 or eq 30, for instance), A and B are nonuniversal constants, and R_g is the gyration radius of the coil. The factor of N^2/R_g^3 is interpreted[83] as a geometric quantity proportional to the number of "contacts" between two chains embedded in a coil correlation volume of radius R_g (which should not be confused with the correlation volume of concentration fluctuations of radius ξ with[32] $\xi \gg R_g$ near T_c). Assuming Gaussian coils, $R_g = \sigma N^{1/2}/6$ where σ is the segment length of the coils; eq 35 can be written as

$$\chi_{eff}(T)/\chi_0(T) = A/\{1 + (N/N_0)^{1/2}\}, \quad N_0 \equiv (\sigma/6)^6 B^{-2} \quad (36)$$

Thus eqs 35 and 36 imply a smooth decrease of $\chi_{eff}/\chi_0(T)$ from a constant for $N \ll N_0$ to a variation $\chi_{eff}/\chi_0(T) \propto N^{-1/2}$ for $N \gg N_0$ (Figure 12a). Although eqs 35 and 36 are a simplification in comparison with the full expression quoted in ref 51, numerical calculations using the latter yield results (Figures 7 and 8 of ref 51) very similar to those in Figure 12a. In contrast, the simulation data show a very different behavior (Figure 12b). To understand fully the meaning of Figure 12, one has to pinpoint what exactly the differences between Flory's mean-field theory and the Schweizer–Curro RISM-MSA theory are. In both theories the *effective* χ parameter χ_{eff} at the spinodal is given through the vanishing of the inverse structure via eq 31, i.e., $\chi_{eff}(T_c) \sim N^{-1}$ in both theories. Also common

for both theories is that $\chi_0(T) \sim \epsilon/k_BT$, i.e., eq 29 or eq 30. The *difference* between the theories is that in Flory's theory it follows that $\chi_0(T) = 2/N(1 - \phi_v) = \chi_{eff}(T_c)$, implying that $\chi_{eff}(T_c)/\chi_0(T_c) = 1$ and $T_c \sim N$, while in the RISM-MSA theory this ratio is always given by eq 36, implying that $T_c \sim \sqrt{N}$ for $N \gg N_0$ when evaluated at $T = T_c$.

All this is summarized in the following equation, where "const" means any quantity independent of N and T:

$$\text{const}\ \frac{k_BT_c}{N\epsilon} = \frac{\chi_{eff}(T_c)}{\chi_0(T_c)} = \begin{cases} 1\ \text{(Flory)} \\ \dfrac{A}{1+\sqrt{N/N_0}} \xrightarrow{N \gg N_0} \dfrac{\text{const}}{\sqrt{N}}\ \text{(Schweizer–Curro)} \end{cases}$$

As emphasized above, the first equality holds in both theories. Therefore, by plotting the simulation data as in Figure 12b, the two theories clearly can be distinguished. Unfortunately, there is a *qualitative discrepancy* between parts a and b of Figure 12; the simulation data in Figure 12b show a slight decrease of T_c/N for very small $N \lesssim 32$ and then settle down to an exactly horizontal straight line. In fact, as pointed out in our preliminary paper,[66] an excellent fit for all N is provided by the simple formula

$$k_BT_c/\epsilon = 2.15N + 1.35 \tag{37}$$

which is of the same type as in Flory–Huggins theory,[6] with two modifications:

(i) There is an additive constant independent of N which physically can be readily interpreted as a correction due to free chain ends (there are more neighboring monomers from other chains available for end monomers than for monomers in the chain interior). (i) The prefactor 2.15 in eq 37 is much less than that one would expect from 29, putting $\chi(T_c) = 2\phi z\epsilon/(k_BT_c) = 2/N$ which for $\phi = 1/2$ would yield

$$k_BT_c/\epsilon = zN\phi \approx 7N \tag{38}$$

where in the last step we have used the effective coordination number of our model, $z \approx 14$ (this can be obtained by counting the monomers that contribute to the first peak of the radial distribution function; see ref 59).

Of course, the discrepancy between parts c and b of Figure 12 could also mean that in the simulation the range of N/N_0 shown in Figure 12a has not yet been reached at all; e.g., if $N = 100$ would correspond to $(N_0/N)^{1/2} = 5$, there would no longer be a contradiction to eq 36. However, this would imply $N_0 = 2500$, and then an explanation for the large value of this crossover chain length N_0 would be needed. In addition, Figure 12a shows that even the region $N \gg N_0$ must be reached to verify the predicted asymptotic behavior $T_c \propto \sqrt{N}$: this prediction would then be very hard to verify experimentally as well. Since "the question whether the nonclassical predictions are somehow an artifact of the MSA (mean spherical approximation) closure of the RISM (reference interaction site model integral equation theory) equations"[51] is not ultimately answered, more work on this question is certainly desirable.

4. Critical Exponents and Critical Amplitudes

In section 2, we have already described how T_c can be estimated unbiased by the problem of estimating other critical properties. In the present section, we return to the expressions of finite-size scaling theory for the moments of the order parameter distribution (eqs 17 and 18) and discuss how these expressions are efficiently used for the estimation of critical exponents contained in them. First we restrict attention to the sufficiently small regime of $N|t|$ (so that the crossover from Ising to mean-field behavior, to be described by inclusion of this variable, is disregarded at the moment).

We begin by noting that the function U_{ij}^{kl} (eq 23) and $kl = ij$ has the form

$$U_{ij}^{kl}(L,t,\mu) = \tilde{U}(L^{1/\nu}t, L^{\beta\delta/\nu}) \tag{39}$$

and emphasize that for any lattice system with all linear dimensions finite (and equal to L) all thermal averages are analytic functions of t and μ, even at the critical point (t=0,μ=0) of the bulk system.[62-64] Therefore for small $|t|$ and $|\mu|$ we may expand eq 39 as

$$U_{ij}^{kl} = U^* + xL^{1/\nu}t + yL^{\beta\delta/\nu}\mu + ... \tag{40}$$

where the constants U^*, x, and y depend on the choice of moment ratio (ij,kl), of course. Equation 40 implies that along the temperature axis ($\mu = 0$)

$$\left.\frac{dU_{ij}^{kl}(L_2,t,0)}{dU_{ij}^{kl}(L_1,t,0)}\right|_{U^*} \approx \frac{U_{ij}^{kl}(L_2,t,0) - U^*}{U_{ij}^{kl}(L_1,t,0) - U^*} = (L_2/L_1)^{1/\nu} \tag{41}$$

and similarly along the critical isotherm ($t = 0$)

$$\left.\frac{dU_{ij}^{kl}(L_2,0,\mu)}{dU_{ij}^{kl}(L_1,0,\mu)}\right|_{U^*} \approx \frac{U_{ij}^{kl}(L_2,0,\mu) - U^*}{U_{ij}^{kl}(L_1,0,\mu) - U^*} = (L_2/L_1)^{\beta\delta/\nu} \tag{42}$$

Thus from the slope of a plot of $U_{ij}^{kl}(L_2,t,0)$ vs $U_{ij}^{kl}(L_1,t,0)$ at $t = 0$ the exponent $1/\nu$ can be estimated,[64,65] and from the slope of a plot of $U_{ij}^{kl}(L_2,0,\mu)$ vs $U_{ij}^{kl}(L_1,0,\mu)$ the exponent $\beta\delta/\nu$ can be estimated. From the function W_k, for even k, defined as[64,65]

$$W_k(L_2,L_1,t,\mu) \equiv -\ln\left(\frac{\langle m^k\rangle_{t,\mu,L_2}}{\langle m^k\rangle_{t,\mu,L_1}}\right)/(\ln L_2/L_1) \tag{43}$$

one obtains (eq 17)

$$W_k(L_2,L_1,0,0) = k\beta/\nu \tag{44}$$

and the same result follows for odd k by using $\langle|m|^k\rangle$ instead of $\langle m^k\rangle$ in eq 43. Since the exponents β, ν, and δ are not independent of each other but related via the hyperscaling law[44,77]

$$d\ (=3) = \beta\delta/\nu + \beta/\nu \tag{45}$$

eqs 41 and 44 allow numerous consistency checks (note that several combinations of L_2 and L_1 are possible with our data, and several choices of k in eq 44 are possible although the accuracy gets worse with higher k). Figure 13 gives an example for $N = 16$, 32, and 256. Since the total number of chains in our lattices is rather small (of order 10^2, as discussed in section 2), it is clear that corrections to finite size scaling are quite important for the lattice sizes shown, unlike for the nearest-neighbor Ising model.[61,64] Therefore, the unique intersection point can be estimated only via some scatter, $U^* \approx 1.24 \pm 0.02$, and a similar scatter results for the corresponding exponent estimate $1/\nu$ (Table I). For $N = 256$, we have discarded the combination $(L_2,L_1) = (80,64)$, since there the intersection corresponds to a temperature too far off the estimated critical temperature. Similar problems due to corrections to scaling (and insufficient statistics) occur when one considers the temperature dependence of the

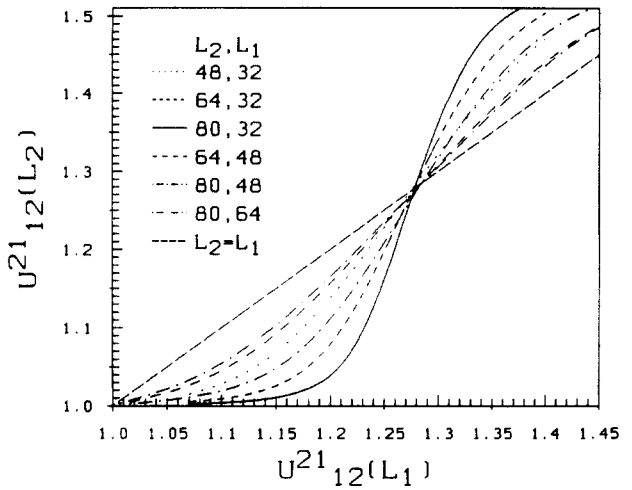

Figure 13. Plot of $U_{12}^{21}(L_2,t,0)$ vs $U_{12}^{21}(L_1,t,0)$ for $N = 64$ (other examples can be found in ref 65). Various curves indicate different choices of (L_2,L_1) as indicated in the figure. Note that finite-size scaling theory implies that these curves should intersect the broken straight line ordinate y = abscissa x all at a unique, universal point $x = y = U^*$, which is independent of L_2, L_1, and N.

functions W_1 and W_2 (Figure 14): at T_c they should intersect in a unique point $W_1 = \beta/\nu$ or $W_2 = 2\beta/\nu$, respectively. Again there is a scatter of a few percent, partly systematic (too small lattices) and partly due to insufficient statistics. Thus the present data do not yet allow a systematic extrapolation of the exponent estimates in order to eliminate corrections to finite-size scaling, unlike recent high precision work for the Ising model.[84] In order to reach a comparable accuracy for polymers, significantly larger lattices and, at the same time, better statistics would be needed: this is out of reach still even with the present day supercomputers such as CRAY-YMP, on which the present study was performed. The drastic differences in the computational effort become clear by noting that a whole chain corresponds to only one spin in the corresponding Ising system.

In spite of these rather large error bars for the critical exponents, the data collected in Table I do display a rather clear trend as a function of chain length: for $N = 16$ and 32 there is very good agreement with the Ising values, while for $N = 64$ and 128 some deviations gradually seem to set in, and for $N = 256$ the "effective exponents" seem to be halfway in between the Ising and the mean-field value. In this context, one must note the complication that for a system that exhibits the critical behavior of mean-field theory one does not have eqs 10, 16–18, and 39 with the Landau mean-field exponents (eq 21), but rather there holds a different form of finite-size scaling, namely (note that this holds for general dimensionality d)[85]

$$P(m) = n^{1/4}\tilde{P}(n^{1/2}t,n^{3/4}\mu,n^{1/4}m) \tag{46}$$

where $\tilde{P}$ is a scaling function different from the scaling function $\tilde{P}$ in eq 10. Equations 17, 18, and 39 in the mean-field limit get replaced by

$$\langle m^k\rangle = n^{-k/4}\tilde{f}_k(n^{1/2}t,n^{3/4}\mu) \tag{47a}$$

$$\langle m^k\rangle = n^{-k/4}\tilde{f}_k'(n^{1/2}t,n^{3/4}\mu) \tag{47b}$$

and {remember that $n = \phi L^d/(2^d N)$}

$$U_{ij}^{kl}(Lt,\mu) = \tilde{U}(L^{d/2}t,L^{3d/4}\mu), \quad ij = kl \tag{48}$$

Thus the analysis explained in eqs 40–44 holds analogously, but the exponents $1/\nu$, $\beta\delta/\nu$, and β/ν get replaced by $d/2$, $3d/4$, and $d/4$, respectively. These exponents replacing the standard exponents in a finite-size scaling analysis are included in the line for the "mean-field" entry of Table I.

The physical reason for this complication is that the mean-field exponents (eq 21) manifestly do not satisfy the hyperscaling relation (eq 45) apart from $d = d^* = 4$ dimensions. Standard finite-size scaling is built on the validity of hyperscaling, however.[85] Both the scaling behavior of eqs 10, 17, 18, and 39 and that of eqs 46–48 can be understood as special cases of the general formula[65,85]

$$P(m) = n^{\beta/(\gamma+2\beta)}\tilde{P}(n^{1/(\gamma+2\beta)}t,n^{(\gamma+\beta)/(\gamma+2\beta)}\mu,n^{\beta/(\gamma+2\beta)}m) \tag{49}$$

If hyperscaling (eq 45) holds, eq 49 reduces to eq 10; if one instead uses the mean-field exponents (eq 21) in eq 49, one obtains eq 46. Observe that the difference between Ising and mean field is only 5.7% of the Ising value for the first exponent combination and therefore hardly detectable with the available statistics. For the second measured exponent however this difference is 47%, and a trend toward mean field for long chains can clearly be seen.

On the other hand, eq 10 contains also the extra variable $N|t|^{(4-d)/(d-2)}$ intended to describe the crossover from Ising behavior for small $N|t|^{(4-d)/(d-2)}$ to mean-field behavior for large $N|t|^{(4-d)/(d-2)}$: while so far this variable was neglected, we now show the implications of eq 10 when we require that it reduces to eq 46 in the limit $N|t|^{(4-d)/(d-2)} \to \infty$. This can happen only if the function $\tilde{P}$ in eq 10 for large $z_4 = N|t|^{(4-d)/(d-2)}$ acquires a singular dependence on its argument z_4 such that in the considered limit the right scaling powers appear. We thus make the ansatz in terms of the scaling variables z_1, z_2, z_3, and {instead of z_4 it is convenient to use the equivalent variable $\zeta = N^{(4-d)/(d-2)}t \equiv N^{\epsilon}t$}

$$P(m)\,dm = P(z_1,z_2,z_3,z_4)\,d\zeta \underset{z_4 \gg 1}{\to} \tilde{P}(z_1^{x_1}\zeta^{y_1},z_2 z_1^{x_2}\zeta^{y_2},z_3 z_1^{x_3}\zeta^{y_3})\, z_1^{x_3}\zeta^{y_3}\,dz_3 \tag{50}$$

Here exponenets x_1, y_1, x_2, y_2, x_3, and y_3 are introduced ad hoc and have to be determined such that the arguments of the scaling function $\tilde{P}$ in eq 50 (which represents the mean-field limit) coincide with those of eq 46. Thus we must have

$$n^{1/2}t = z_1^{x_1}\zeta^{y_1} = c_1^{x_1}n^{x_1/(d\nu)}t^{x_1}N^{\epsilon y_1}t^{y_1} \tag{51a}$$

$$n^{3/4}\mu = z_2 z_1^{x_2}\zeta^{y_2} = c_2 n^{\beta\delta/(d\nu)}\mu c_1^{x_2}n^{x_2/(d\nu)}t^{x_2}N^{\epsilon y_2}t^{y_2} \tag{51b}$$

$$n^{1/4}m = z_3 z_1^{x_3}\zeta^{y_3} = c_3 n^{\beta/(d\nu)}m c_1^{x_3}n^{x_3/(d\nu)}t^{x_3}N^{\epsilon y_3}t^{y_3} \tag{51c}$$

Equating the exponents of n and t on both sides of these equations yields the exponents x_1, y_1, x_2, y_2, x_3, and y_3:

$$x_1 = d\nu/2, \quad y_1 = 1 - x_1 = 1 - d\nu/2 \tag{52a}$$

$$x_2 = 3d\nu/4 - \beta\delta, \quad y_2 = -x_2 = \beta\delta - 3d\nu/4 \tag{52b}$$

$$x_3 = d\nu/4 - \beta, \quad y_3 = -x_3 = \beta - d\nu/4 \tag{52c}$$

First of all, this consideration shows that there is no contradiction between eq 10 and eq 46 in spite of the different scaling powers of n that appear in both equations: due to the extra variable z_4 in eq 10, one may reduce eq 10 to eq 46 for large z_4, by the special combination of arguments involving z_4 of ζ written in eq 50. A further interesting consequence of this crossover description is that in the considered large N limit predictions are

Table I
Critical Temperatures, Effective Critical Exponents, and Effective Critical Amplitudes

N	k_BT_c/ϵ	$d/(\gamma+2\beta)$	$\beta d/(\gamma+2\beta)$	$\hat{B}_{eff}$	$\hat{D}_{eff}$	$\hat{C}_{eff}^-$	$\hat{C}_{eff}^+$	$\hat{C}_{\mu,eff}$	$\hat{C}_{m,eff}$
Ising model		$1/\nu = 1.59$	$\beta/\nu = 0.51$						
16	36.15 ● 0.20	1.56 ● 0.03	0.50 ± 0.02	1.38	0.995	0.20	0.96	0.40	0.59
32	69.35 ● 0.30	1.59 ± 0.03	0.505 ± 0.02	1.365	0.98	0.184	0.86	0.37	0.57
64	138.9 ± 0.2	1.53 ± 0.03	0.565 ± 0.02	1.39	0.964	0.24	0.82	0.43	0.56
128	277.7 ± 0.6	1.58 ± 0.04	0.561 ± 0.03	1.29	0.956	0.27	0.72	0.45	0.50
256	540.6 ± 10	1.53 ± 0.04	0.623 ± 0.04	1.51	1.03	0.25	0.85	0.491	0.76
mean field		$d/2 = 1.5$	$d/4 = 0.75$						

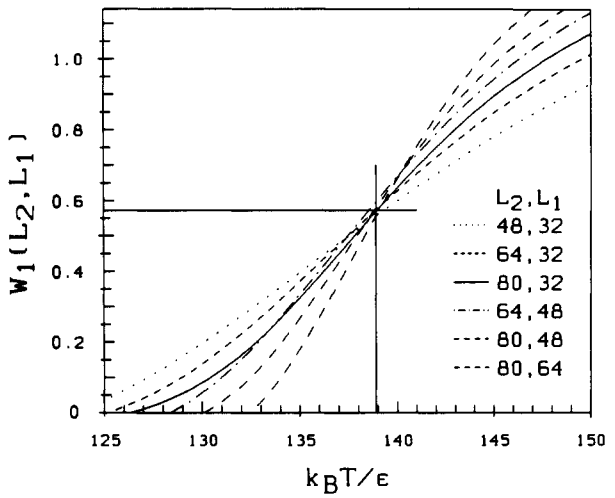

Figure 14. Plot of $W_1(L_2,L_1,t,0)$ versus k_BT/ϵ for $N = 64$. Different pairs (L_2,L_1) are shown as dotted, dashed, solid, and dash-dotted curves, etc., as indicated in the figure. The cross lines show the best estimate of T_c. Note that the effective exponent β/ν is in between the Ising and the mean-field prediction.

obtained for the N dependence of the scale factors c_1, c_2, and c_3 in eq 10, that so far has not yet been specified. This is seen by the fact that in the mean-field limit in terms of our reduced variables t, μ, and m there is no N dependence left. Therefore, no scale factors were needed for the three arguments in eq 46 and on the left-hand side of eq 51a–c, which implies that the N dependence on the right-hand side of these equations also must cancel out:

$$c_1^{x_1}N^{\epsilon y_1} = 1, \quad c_1 = N^{-\epsilon y_1/x_1} = N^{-(2-d\nu)\epsilon/(d\nu)} \tag{53a}$$

$$c_2c_1^{x_2}N^{\epsilon y_2} = 1, \quad c_2 = c_1^{-x_2}N^{-\epsilon y_2} = N^{(3d\nu-4\beta\delta)\epsilon/(2d\nu)} \tag{53b}$$

$$c_3c_1^{x_3}N^{\epsilon y_3} = 1, \quad c_3 = c_1^{-x_3}N^{-\epsilon y_3} = N^{(d\nu-4\beta)\epsilon/(2d\nu)} \tag{53c}$$

These results for the N dependence of the scale factors of the finite-size scaling function $\tilde{P}$ (eq 10) imply a singular N dependence of the critical amplitudes $\hat{B}$, $\hat{D}$, $\hat{C}^{\pm}$, etc. (eqs 11–15), as well. E.g., from eqs 25 and 26 we conclude that

$$\langle|m|\rangle = c_3^{-1}n^{-\beta/d\nu}\tilde{f}_1'(z_1) \underset{z_1\to-\infty}{\to} \hat{B}'c_3^{-1}c_1^{\beta}(-t)^{\beta} \tag{54}$$

where $\hat{B}$ is a constant characterizing the limiting behavior of a universal scaling function and hence cannot exhibit an N dependence anymore. Therefore, comparing eqs 11 and 54 and using eq 53a,c yield the N dependence of the critical amplitude $\hat{B}$

$$\hat{B} \propto N^{(\beta-1/2)\epsilon} \approx N^{-0.176} \tag{55}$$

where in the last step eq 20 for $d = 3$ was used. By similar reasoning as in eqs 25, 26, 54, and 55 we obtain from eqs 12, 17, 53, and 20 that

$$\hat{D} \propto N^{(3/\delta-1)\epsilon/2} \approx N^{-0.189} \tag{56}$$

and from eqs 14, 15, 17, 53, and 20

$$\hat{C}^{\pm} \propto N^{(1-\gamma)\epsilon} \approx N^{-0.239} \tag{57}$$

At this point, it becomes convenient to define another critical amplitude $\hat{C}_\mu$ describing the response function $k_BT_c\chi_m$ (eqs 14 and 15) at T_c in the limit $\mu \to 0$, $t \equiv 0$

$$k_BT_c\chi_m(t=0) = \hat{C}_\mu\mu^{-\gamma/(\beta\delta)}, \quad \mu \to 0^+ \tag{58}$$

for which we analogously obtain

$$\hat{C}_\mu \propto N^{(1-3\gamma/(2\beta\delta))\epsilon} \approx N^{-0.189} \tag{59}$$

While eqs 56 and 57 have been obtained previously[41] by a crossover scaling assumption for bulk quantities not relying on finite-size scaling,[86] eq 59 is new. Equations 58 and 59 are of interest because combining them with eqs 12 and 56 we also obtain

$$k_BT_c\chi_m(t=0) = \hat{C}_m\langle m\rangle^{-\gamma/\beta}, \quad T = T_c \tag{60}$$

with

$$\hat{C}_m = \hat{C}_\mu(\hat{D})^{\gamma/\beta} \propto N^{(1-\gamma/(2\beta))\epsilon} \approx N^{-0.912} \tag{61}$$

Since χ_m is related to $S_{coll}(\vec{k}\to 0)$ (eq 14), one could measure χ_m at T_c by careful scattering experiments as a function of the composition of the blend. Such an experiment would be interesting, since the exponent $\gamma/\beta \approx 3.82$ in eq 60 is very different from its mean-field value 2, and also there is a strong N dependence of the corresponding critical amplitude (eq 61).

Now an additional merit of our analysis of crossover scaling in the context of finite-size scaling is that it readily yields predictions for the N dependence of amplitude prefactors characterizing the critical size dependence of various quantities at T_c. In fact, from eqs 17, 18 and 53 we immediately conclude

$$\langle|m|\rangle_{t=0,\mu=0} = c_3^{-1}n^{-\beta/d\nu}\tilde{f}_k'(0,0,0) \propto N^{(4\beta-d\nu)\epsilon/(2d\nu)}n^{-\beta/d\nu}$$
$$\propto N^{[2\beta+\epsilon(4\beta-d\nu)]/(2d\nu)}L^{-\beta/\nu} \approx N^{0.015}L^{-0.515} \tag{62a}$$

$$k_\beta T_c\chi_m|_{t=0,\mu=0} = c_3^{-2}n^{\gamma/d\nu}\{\tilde{f}_2(0,0,0) - [\tilde{f}_1'(0,0,0)]^2\} \propto$$
$$N^{(4\beta-d\nu)\epsilon/d\nu}n^{\gamma/d\nu}$$
$$\propto N^{[-\gamma+\epsilon(4\beta-d\nu)]/d\nu}L^{\gamma/\nu} \approx N^{-1.061}L^{1.97} \tag{62b}$$

In contrast, the corresponding mean-field predictions would be (eqs 19 and 47a,b)

$$\langle|m|\rangle_{t=0,\mu=0} = L^{-d/4}\tilde{f}_1'(0,0) \propto L^{-3/4} \tag{63a}$$

$$k_BT_c\chi_m|_{t=0,\mu=0} = L^{d/2}\{\tilde{f}_2(0,0) - [\tilde{f}_{1'}(0,0)]^2\} \propto L^{3/2} \tag{63b}$$

where no powers of N appear. Also the maximum value $k_BT_c\chi_m^{max}(\mu=0)$ which can be estimated independent of T_c scales in the same way as $k_BT_c\chi_m(t=0,\mu=0)$. Of course, both eqs 62 and 63 have been derived as limiting forms

of the same expression (eq 10): Equation 62 resulted by taking the limits $t \to 0$ and $\mu \to 0$ first and then the limit large N is considered, while eq 63 results from first taking the limit $N \to \infty$. There occurs a smooth crossover between both limits. This crossover is conveniently studied when we eliminate from the first variable z_1 of eq 10 the dependence on t by multiplying z_1 with a suitable power of z_4

$$P(m) = N^{(1/2-2\beta/d\nu)\epsilon} n^{\beta/d\nu} \tilde{P}''(n^{1/d\nu} N^{-2\epsilon/d\nu}, c_2 n^{\beta\delta/d\nu}\mu, N^{(1/2-2\beta/d\nu)\epsilon} n^{\beta/d\nu} m, N|t|^{1/\epsilon}) \quad (64a)$$

where $\tilde{P}''$ is a suitable scaling function. Writing n as $n = \phi L^d/(2^d N) = \text{const}\ L^d/N$ and then eliminating the L dependences in the prefactor and in the second and third argument of $\tilde{P}''$ via multiplications with suitable powers of the first argument of $\tilde{P}''$, one arrives after some algebra at a more aesthetic crossover finite-size scaling form for the order parameter distribution

$$P(m) = N^{\epsilon/2} \tilde{P}(N^{-(2\epsilon+1)/d} L, N^{\epsilon} t, N^{3\epsilon/2}\mu) \quad (64b)$$

where $\tilde{P}$ is again a scaling function. The first moment of $P(m)$ for $t = 0$, $\mu = 0$ now reads

$$\langle |m| \rangle = N^{-\epsilon/2} \tilde{m}(N^{-(2\epsilon+1)/d} L) \quad (65a)$$

and similarly the maximum value of the response function is found to scale as

$$k_B T_c \chi_m^{\max}(\mu=0) \propto k_B T_c \chi_m(t=0,\mu=0) = L^d N^{-(\epsilon+1)} \tilde{\chi}(N^{-(2\epsilon+1)/d} L) \quad (65b)$$

Here again $\tilde{m}$ and $\tilde{\chi}$ are scaling functions.

These considerations are now tested by the data of the present simulations in Figures 15–17. It is seen that the size dependence of both $\langle |m| \rangle_{t=0,\mu=0}$ and $k_B T_c \chi_m^{\max}(\mu=0)$ is in fact compatible with a power law behavior, as expected. On the log–log plots of Figure 15, power laws show up as straight lines, the slope being the associated exponent. Of course, since only for each N a few values of L are available, the data always seem compatible with straight lines, even if we are between the limiting cases described by eq 62 or eq 63, respectively. The effective exponents following from the slopes of the straight lines in Figure 15a would be $(\beta/\nu)_{\text{eff}} = 0.508$ ($N = 16$), 0.506 ($N = 32$), 0.577 ($N = 64$), 0.567 ($N = 128$), and 0.61 ($N = 256$), respectively. This is in reasonable agreement with the determination from the data for W_1 (Table I). Implying a scaling relation $\gamma/\nu = d - 2\beta/\nu$, Figure 15b can be used as well to estimate $(\beta/\nu)_{\text{eff}}$, which yields $(\beta/\nu)_{\text{eff}} = 0.503$ ($N = 16$), 0.5 ($N = 32$), 0.544 ($N = 64$), 0.55 ($N = 128$), and 0.57 ($N = 256$). As expected, for short chains we observe the universal Ising exponents, and then all these numbers are in very good agreement with each other. However, in the crossover region these effective exponents have only a meaning in terms of the slopes of the crossover scaling functions $\tilde{f}(x)$ and $\tilde{F}(x)$ at the respective values of x, and thus different ways of estimation yield somewhat different estimates in the crossover region.

A direct test of eq 65 is performed by a scaling plot $\langle |m| \rangle_{t=0,\mu=0} N^{1/2}$ vs $x = LN^{-(2\epsilon+1)/d}$ ($= L/N$ in $d = 3$) and of $N^2 k_B T_c \chi_m^{\max}(\mu=0) L^{-3}$ vs x (Figure 16). Given the statistical errors of our data and the fact that both corrections to thermodynamic scaling and to finite-size scaling are ignored throughout, the "data collapsing" in Figure 16a,b is satisfactory.

An attractive alternative check of this idea outlined in eqs 50–61, which also in principle is feasible with data from real mixtures, is a study of the chain-length dependence of critical amplitudes (eqs 55–61). However, it is well-known that an accurate estimation of critical amplitudes is even more difficult than the estimation of

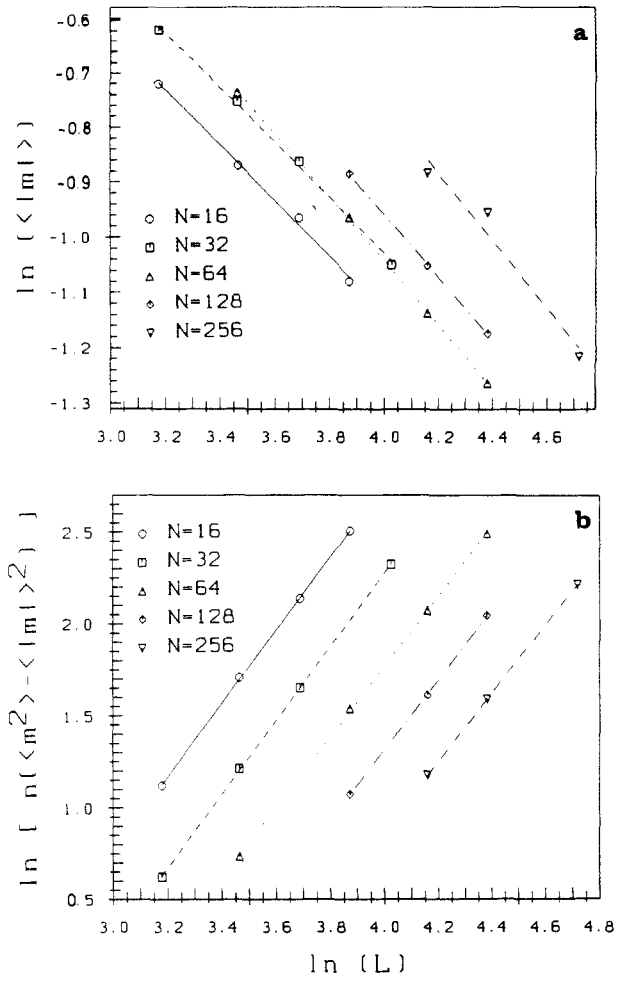

Figure 15. log–log plot of $\langle |m| \rangle_{t=0,\mu=0}$ (a) and $k_B T \chi_m^{\max}(\mu=0)$ (b) versus L. Different symbols represent the various chain lengths used, as indicated in the figure.

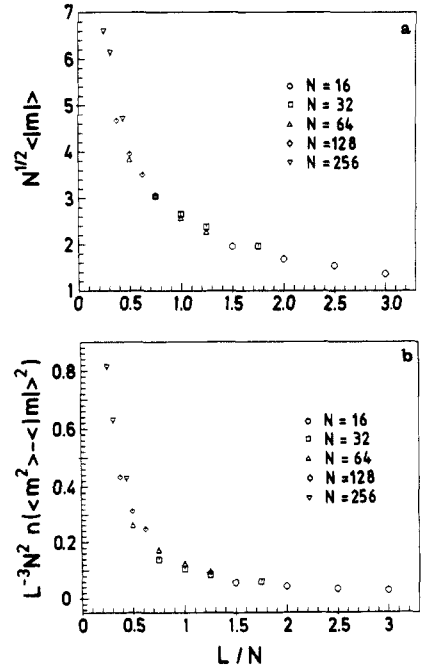

Figure 16. Evidence for crossover finite-size scaling by plotting $\langle |m| \rangle_{t=0,\mu=0} N^{1/2}$ (a) and $k_B T \chi_m^{\max}(\mu=0) N^2 L^{-3}$ (b) vs L/N. Different symbols represent the various chain lengths used, as indicated in the figure.

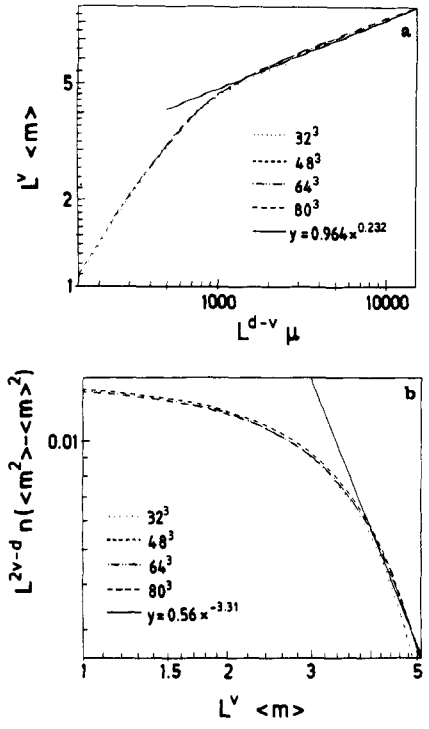

Figure 17. Scaled order parameter for $N = 64$, $\mu > 0$, $T = T_c$ (a) and response functional $T = T_c$, $\langle m\rangle \pm 0$ (b) plotted vs the respective scaling variables. Different curves show the various choices of L, as indicated in the figure. The straight line shows the asymptotic behavior; intercept of this straight line with the ordinate axis yields the effective critical amplitude. Note that the slope of this straight line is fixed by the choice of the effective exponents β.

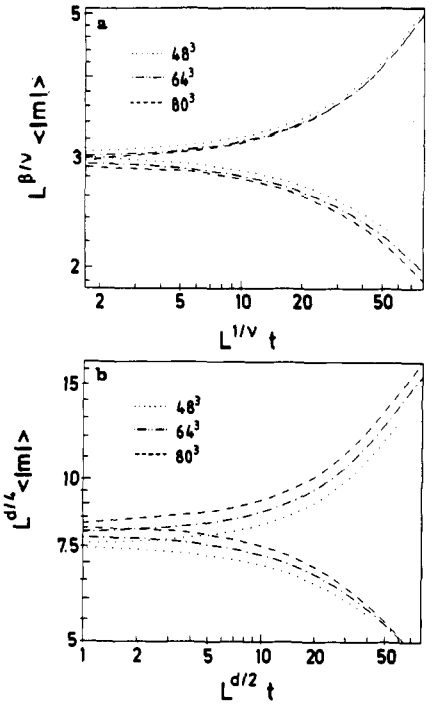

Figure 18. (a) Scaled plot of $L^{\beta/\nu}\langle|m|\rangle$ vs $L^{1/\nu}$ for $N = 128$, using $k_BT/\epsilon = 277.7$ and the Ising exponents (eq 20). Three different curves show the three values of L available. (b) Same as a, but using mean-field scaling (eq 47). Obviously the scaling is worse; the best scaling is obtained with "effective" intermediate exponents (Figure 5).

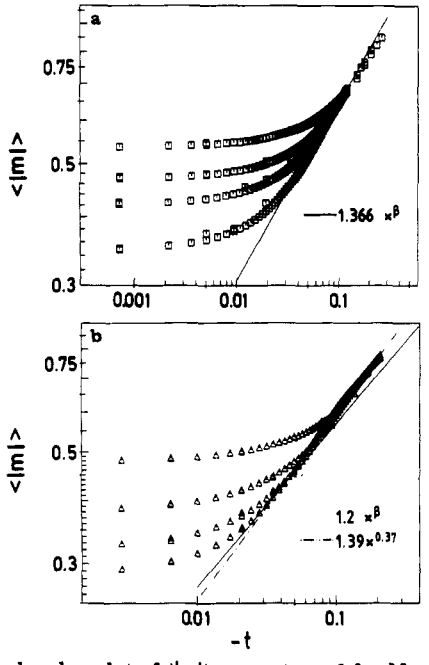

Figure 19. log–log plot of $\langle|m|\rangle$ vs $-t$ at $\mu = 0$ for $N = 32$ (a) and $N = 64$ (b). A broken straight line indicates a possible asymptotic power law for $t \to 0$, using always the Ising exponent $\beta = 0.324$. Note that for large N the data deviate from this power law to larger values of $\langle|m|\rangle$, for not too large $|t|$, because then mean-field critical behavior ($\beta^{MF} = 0.5$) starts to set in.

critical exponents: small errors in the estimate of the exponents get magnified to a large error in the corresponding amplitude. Thus the critical amplitudes obtained from fits such as those shown in Figures 5 and 17 and included fully in Table I are effective amplitudes only, and since part of the crossover is included in a change of the corresponding effective exponent, it is no surprise that these effective critical amplitudes do not satisfy the predictions (eqs 55–61) and even exhibit a nonmonotonic dependence with chain length. Thus one might try to follow the procedure of ref 41 and use the Ising exponents (eq 20), which should inevitably describe the asymptotic critical behavior as $\mu \to 0$, $t \to 0$, as an input for the finite-size scaling plot. However, for large N where the crossover problems occur one sees distinct systematic deviations of the various curves from each other (Figure 18a) instead of a reasonable data collapsing: unambiguous estimation of critical amplitudes there is very difficult. Assuming mean-field scaling (Figure 18a) the situation is even worse.

In this situation, we have found it most reliable to estimate the critical amplitudes from plots of the raw data for different system sizes (Figure 19) and fitting a straight line with the theoretical slope (eq 20) to that part of the data where different system sizes overlap. Critical amplitudes of the order parameter obtained in this way are very inaccurate for large N, but now the variation with N is monotonic and consistent with the expected power laws (eqs 55 and 56); see Figure 20. Unfortunately, the critical amplitudes of the response function cannot be estimate at all by such methods with meaningful accuracy. While Figure 20 shows that for large enough N the data are possibly compatible with the crossover scaling theory outlined above, the large error bars of the critical amplitudes for large N prevent us from making very definitive statements. However, the present results again indicate that the different behavior for small N already seen in ref 41 is not the asymptotic behavior for large N, and thus the present study at least indirectly corroborates the conclusion of refs 45, 46, 53, and 54 that for lattices containing many vacancies there is a reduction of χ_{eff} due to the formation of excluded-volume "blobs"[9] on small length scales, and thus the behavior for small N must be interpreted in terms of a theory describing unmixing of two polymers in a semidiluted solution of a common solvent.[45,46] This case is outside of interest here. We

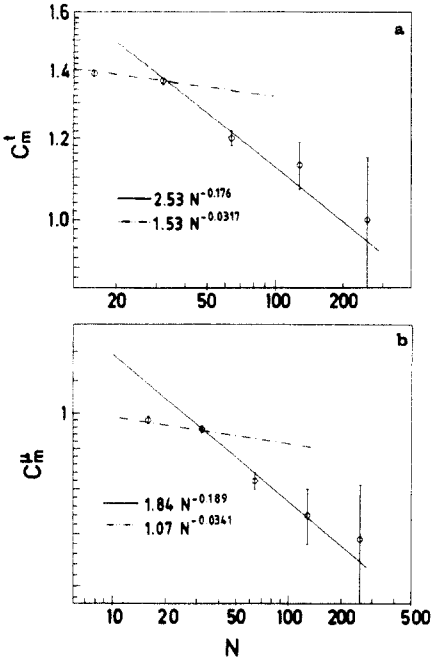

Figure 20. log–log plot of critical amplitude $\hat{B}$ (a) and $\hat{D}$ (b) vs N. Straight lines are best fits to all data with $N \geq 32$, using the theoretical exponents in eqs 55 and 56, respectively. Dash-dotted straight lines show straight lines using the modified exponents proposed by Joanny et al.[45,46] for the semidilute regime.

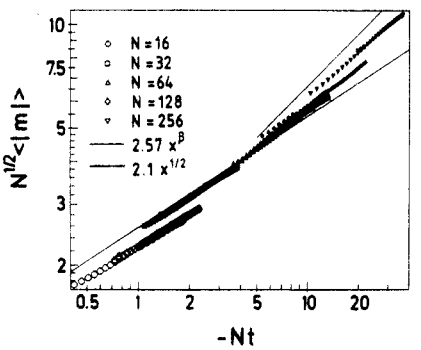

Figure 21. log–log plot of $N^{1/2}\langle|m|\rangle$ vs $N|t|$ to check for the validity of crossover scaling. Different symbols show various chain lengths N, as indicated. Only such data were included for which the L dependence was negligible. Straight lines indicate the Ising power law $\{\propto (N|t|)^{1/2}$, valid for $N|t| \lesssim 1\}$ and the mean-field power law $\{\propto (N|t|)^{1/2}$, valid for $N|t| \gg 1\}$.

emphasize that a crossover scaling plot of bulk ($L \to \infty$) order parameter data for $N = 32$ to $N = 128$ scales reasonably well (Figure 21); only the data for $N = 16$ are distinctly off. In ref 41, only data for $N = 4$, 8, 16, and 32 have been compared in the analogous plot (Figure 12 of ref 41), and these chains probably all were too short to fall in the region where the crossover scaling theory applies. (The motivation for Figure 21 follows from the first moment of the distribution (eq 64b) in the L-independent regime in $d = 3$.) Also in the present case, it is clear that the data for small N fall into the Ising regime ($N|t| \approx$ unity or smaller) or in the crossover regime where neither Ising nor mean-field behavior holds ($N|t| \approx 10$). Substantially larger lattices and longer chains would be needed to reach the regime $N|t| \gtrsim 10^2$ where pure mean-field behavior would set in.

5. Discussion

In the present paper the critical properties of symmetrical polymer mixtures have been investigated by a Monte Carlo study of the bond fluctuation model on the simple cubic lattice, for a volume fraction of occupied sites $\phi = 0.5$. As has been shown in earlier work on the statics and dynamics of this model[60] for homopolymers, this volume fraction corresponds to a dense melt—the structure factor of single chains well follows the Debye function, the gyration radius for $N > 20$ follows the classical law $R_g \sim N^{0.5}$, and the self-diffusion constant D_N depends on N just in the same way as experimental data do, if the entanglement chain length N_e is properly identified.[60] From such comparisons it was concluded that one bond in our model corresponds to about three monomers in polyethylene, which would mean that the chain length range accessible in the present study, $N = 16$ to $N = 256$, roughly corresponds to a degree of polymerization N_P in the range from $N_P \approx 50$ to $N_P = 750$ for real polymers. Thus while our shortest chains clearly correspond to oligomers, the longest chains correspond to values of N_P as are sometimes used in experimental studies,[68,71] although some measurements refer to even much longer chains ($N_P \approx 10^4$).[81,87]

As an interaction between the monomers, we have chosen the most symmetric choice $\epsilon_{AA} = \epsilon_{BB} = -\epsilon_{AB} = -\epsilon$ and choose the range of this interaction such that all possible distances up to $\sqrt{6}$ lattice spacings contribute. Although there are 54 possible distance vectors, one should not erroneously conclude that this is a square well potential with a coordination number of 54; due to the fact that our monomers are large objects blocking a cube of eight neighboring sites for any further occupation (Figure 1), there develop strong correlations at small distances, as evidenced[59] by the radial density distribution function $g(r)$. The above distances are chosen such that the full weight of the first peak of $g(r)$, which corresponds to an effective coordination number $z = 14$ similar to real fluids, is included. Thus our choice of interactions is a truly short-range potential, and hence fluctuations are not suppressed (as they would be if we had chosen a potential of much longer range). This fact is also evident from the clearcut Ising-like critical behavior that is observed in our model for chain lengths $N = 16$ and $N = 32$.

Due to technical advances of the simulation method (use of fast vectorizing programs on supercomputers, histogram analysis, etc.), we have been able to estimate critical temperatures with a high accuracy (Table I) and also (effective) critical exponents and (effective) critical amplitudes. We call these quantities effective because only for small N do we see clearly the Ising behavior, while particularly for $N = 128$ and $N = 256$ exponents somehow intermediate between Ising and Flory–Huggins mean-field behavior have been obtained. Thus the present work corresponds clearly to a range of much larger N_P values than the previous data,[41,42] where only Ising-like behavior was found. We have tried to analyze our data in the framework of a combined finite-size scaling and crossover scaling analysis, which has been formulated in the present paper for the first time. Although our data are compatible with such an analysis, they certainly do not prove it: both much larger lattice linear dimensions L and somewhat longer chain lengths N would be needed for a really convincing test of these new concepts. In any case, the present work indicates how the problems with crossover scaling encountered previously[41] can be resolved. At this point we comment on the problems with universal amplitude ratios[88] encountered previously.[41,42] The predicted values are for the universality class of the three-dimensional Ising model,[88] $\hat{C}^+/\hat{C}^- \approx 4.9$ and $R_\chi = \Gamma D_c B^{\delta-1} \approx 1.6$ (Γ, B, and D_c being critical amplitudes in Ising model language[88]). In our notation, $R_\chi = (1/2)(\hat{C}^+/\hat{B})(\hat{B}/\hat{D})^\delta$. Using the data from Table I for $N = 16$ where the exponents have their theoretical (Ising) values, we find $\hat{C}^+/\hat{C}^- \approx 4.8$

and $R_\chi \approx 1.68$. Thus, the agreement with the theoretical prediction is excellent! Part (but not all) of the problems found previously[41,42] are due to the fact that their $\hat{C}^+$ was too small by a factor of $1-2/\pi$ {due to the use of $\langle m^2\rangle - \langle|m|\rangle^2$ rather than $\langle m^2\rangle$ to extract the response function above T_c}.

Among the predictions resulting from our work are anomalous exponents of power laws for the N dependence of critical amplitudes. The critical amplitude of the response function {or collective scattering factor $S_{coll}(\vec{k}\to 0)$} both as a function of temperature at $\phi_A = \phi_A^{crit}$ and as function of ϕ_A at $T = T_c$ should be accessible to the experimental test. While the Ising critical exponent for $S_{coll}(\vec{k}\to 0)$, first proposed by Sariban and Binder,[41] now has been seen in several experiments,[67-70] we are not aware of any experiment attempting to verify eqs 57 or 61, respectively. Observation of such a power law would be a direct test of crossover scaling.

A somewhat controversial point is the chain-length dependence of the critical temperature. A naive application of Flory–Huggins theory would relate it to the abovementioned effective coordination number as $k_B T_c/\epsilon = (1/2)zN = 7N$ (in our normalization). Instead we find eq 37, i.e., the prefactor in the relation between T_c and N, is strongly reduced by about a factor of 3, consistent with the findings of refs 41 and 42 for a different model. In addition, there is a correction due to the free ends of the chain. One should not misunderstand this renormalization of χ as done in ref 71, however, where χ_{eff} is extracted from fitting the Flory–Huggins equation to the phase diagram and the chain-length dependence of this χ_{eff} was studied: if we extract χ_{eff} from the simulation data, applying the Flory–Huggins equation, we find a consistency, between the extrapolated critical temperature and the actual one, since their mismatch is only on the order of 1% (Figure 7). However, the effective Flory–Huggins parameter estimated in this way has a spurious concentration dependence (Figure 10b) and a singular temperature dependence (particularly below T_c; see Figure 11).

Thus although there is a significant and nontrivial renormalization of the Flory–Huggins parameter from its naive value ($=z\epsilon/k_BT$ in our normalization) to a significantly smaller and concentration-dependent value, we do not see the dramatic chain-length dependence of this renormalization predicted by the integral equation theory of Schweizer and Curro;[50,51] cf. parts a and b of Figure 12. Of course, one could always argue that even our largest chains are by far shorter than the chracteristic chain length N_0 (eq 36) needed to see their result, $k_bT_c/\epsilon \propto \sqrt{N}$. However, in our opinion the occurrence of such a dramatic reduction of T_c for Gaussian chains is very unplausible: since the density of the monomers of a considered chain in its gyration volume R_g^3 is of order $N/R_g^3 \approx 1/\sqrt{N}$, each monomer of the chain is primarily surrounded by monomers of *other* chains. Hence, the total enthalpy change ΔU involved when we replace this chain (of type A) by a chain of type B is of order ϵN, since each of the N monomers of the chain contributes an enthalpy of order ϵ. On the other hand, the entropy change ΔS involved in A $\leftrightarrow$ B interchanges is of order k_B ln 2 only. Now in all phase transition problems the order of magnitude of T_c can be estimated correctly by putting $\Delta U \approx T_c\Delta S$, which yields $T_c \propto N$. Estimates of this sort fail qualitatively only if the system is at or below its lower critical dimensionality[71] for a phase transition—such as the Ising model in $d = 1$ dimension—which is not the case here. Thus such a strong reduction of T_c due to correlations would not have a precedent in other phase transition problems. Of course, these arguments are qualitative plausibility considerations only, and more work on all these issues—experimental, theoretical, and simulational—is clearly very desirable.

Acknowledgment. H.-P.D. received partial support from the Deutsche Forschungsgemeinschaft under Grant No. Bi 314/3. We are grateful to the Höchstleistungsrechenzentrum (HLRZ) Jülich and the Regionales Hochleistungsrechenzentrum Kaiserlautern (RHRK) for generous grants of computer time on the CRAY-YMP and Fujitsu VP100 vector processors. We also thank Prof. K. Schweizer for helpful correspondence.

References and Notes

(1) Flory, P. J. *J. Chem. Phys.* **1941**, *9*, 660; **1942**, *10*, 51.
(2) Huggins, M. L. *J. Chem. Phys.* **1941**, *9*, 440; *J. Chem. Phys.* **1942**, *46*, 151; *J. Am. Chem. Soc.* **1942**, *64*, 1712.
(3) Staverman, A. J. *Recl. Trav. Chim. Pays-Bas* **1941**, *60*, 640. Staverman, A. J.; Van Santen, J. H. *Recl. Trav. Chim. Pays-Bas* **1941**, *60*, 76.
(4) Guggenheim, E. A. *Proc. R. Soc. (London)* **1945**, *A183*, 203, 231.
(5) Scott, R. L. *J. Chem. Phys.* **1949**, *17*, 279.
(6) Flory, P. J. *Principles of Polymer Chemistry*; Cornell University Press: Ithaca, NY, 1953.
(7) Tompa, H. *Polymer Solutions*; Butterworths: London, 1956.
(8) Koningsveld, R.; Kleintjens, L. A.; Nies, E. *Croat. Chim. Acta* **1987**, *60*, 53.
(9) de Gennes, P.-G. *Scaling Concepts in Polymer Physics*; Cornell University Press: Itaca, NY, 1979.
(10) Koningsveld, R. *Adv. Colloid Interface Sci.* **1968**, *2*, 151. Koningsveld, R.; Kleintjens, L. A.; Schoffeleers, H. M. *Pure Appl. Chem.* **1974**, *39*, 1.
(11) Zeman, L.; Patterson, D. *Macromolecules* **1972**, *5*, 513.
(12) Sanchez, I. C.; Lacombe, R. J. *J. Phys. Chem.* **1976**, *80*, 2352; *Macromolecules* **1978**, *11*, 1145. Lacombe, R. H.; Sanchez, I. C. *J. Phys. Chem.* **1976**, *80*, 2568.
(13) Sanchez, I. C. *Macromolecules* **1984**, *17*, 967.
(14) Solc, K. *Macromolecules* **1986**, *19*, 1166.
(15) Helfand, E.; Tagami, Y. J. *Polym. Sci.* **1971**, *B9*, 741; *J. Chem. Phys.* **1971**, *56*, 3592; *J. Chem. Phys.* **1972**, *57*, 812. Helfand, E. *J. Chem. Phys.* **1975**, *62*, 999; *J. Chem. Phys.* **1975**, *63*, 2792.
(16) Helfand, E.; Sapse, M. *J. Chem. Phys.* **1975**, *62*, 1327. Helfand, E.; Weber, T. A. *Macromolecules* **1976**, *9*, 311.
(17) Joanny, J. F.; Leibler, L. *J. Phys. (Paris)* **1978**, *39*, 951.
(18) Binder, K.; Frisch, H. L. *Macromolecules* **1984**, *17*, 2928.
(19) Schmidt, I.; Binder, K. *J. Phys. (Paris)* **1985**, *46*, 1631.
(20) Carmesin, I.; Noolandi, J. *Macromolecules* **1989**, *22*, 1689.
(21) Leibler, L. *Macromolecules* **1980**, *13*, 1602.
(22) Hong, K. M.; Noolandi, J. *Macromolecules* **1981**, *14*, 727; *Macromolecules* **1983**, *16*, 1083. Noolandi, J.; Hong, K. M. *Macromolecules* **1982**, *15*, 482; *Macromolecules* **1983**, *16*, 1443.
(23) Helfand, E.; Wasserman, Z. R. *Macromolecules* **1976**, *9*, 879; *Macromolecules* **1978**, *11*, 960.
(24) Semenov, A. N. *Sov. Phys. JETP* **1985**, *61*, 733. Birshtein, T. M.; Zhulina, E. B. *Polymer* **1990**, *31*, 1312.
(25) Kawasaki, K.; Ohta, T. *Macromolecules* **1986**, *19*, 2621. Kawasaki, K.; Ohta, T.; Kohrogu, M. *Macromolecules* **1988**, *21*, 2972.
(26) Fredrickson, G. H.; Helfand, E. *J. Chem. Phys.* **1987**, *87*, 697.
(27) Noolandi, J.; Kavassalis, T. A. In *Molecular Conformation and Dynamics of Macromolecules in Condensed Systems*; Nagasawa, M., Ed.; Elsevier: Amsterdam, The Netherlands, 1988; p 285.
(28) Fredrickson, G. H.; Binder, K. *J. Chem. Phys.* **1989**, *91*, 7265.
(29) Burger, C.; Ruland, W.; Semenov, A. N. *Macromolecules* **1990**, *23*, 3339.
(30) de Gennes, P.-G. *J. Chem. Phys.* **1980**, *72*, 4756.
(31) Pincus, P. *J. Chem. Phys.* **1981**, *75*, 1996.
(32) Binder, K. *J. Chem. Phys.* **1983**, *79*, 6387; *Phys. Rev. A* **1984**, *29*, 341.
(33) Onuki, A. *J. Chem. Phys.* **1986**, *85*, 1122.
(34) Brochard, F.; Jouffroy, J.; Levinson, P. *Macromolecules* **1983**, *16*, 1638; *J. Phys. Lett. (Paris)* **1983**, *4*, L-455.
(35) Kramer, E. J.; Green, P.; Palmstrom, C. *Polymer* **1984**, *25*, 473.
(36) Sillescu, H. *Makromol. Chem., Rapid Commun.* **1984**, *5*, 519; *Makromol. Chem., Rapid Commun.* **1987**, *8*, 393.
(37) Brochard, F.; de Gennes, P.-G. *Europhys. Lett.* **1986**, *1*, 221. Brochard-Wyart, F. C. R. *Acad. Sci. Ser. II (Fr.)* **1987**, *305*, 657.
(38) Akcasu, A. Z.; Benmouna, M.; Benoit, H. *Polymer* **1986**, *27*, 1935. Hess, W.; Akcasu, A. Z. *J. Phys. (Fr.)* **1988**, *49*, 1261.

(39) Binder, K. *Colloid Polym. Sci.* **1987**, *265*, 237. Schichtel, T. E.; Binder, K. *Macromolecules* **1987**, *20*, 1671. Jilge, W.; Carmesin, I.; Kremer, K.; Binder, K. *Macromolecules* **1990**, *23*, 5001.
(40) de Gennes, P.-G. *J. Phys. Lett. (Paris)* **1977**, *38*, L441. Joanny, J. F. *J. Phys. A: Math. Gen.* **1978**, *11*, L117.
(41) Sariban, A.; Binder, K. *J. Chem. Phys.* **1987**, *86*, 5859.
(42) Sariban, A.; Binder, K. *Macromolecules* **1988**, *21*, 711.
(43) Sariban, A.; Binder, K. *Colloid. Polym. Sci.* **1989**, *267*, 469.
(44) Stanley, H. E. *An Introduction to Phase Transitions and Critical Phenomena*; Oxford University Press: Oxford, U.K., 1971.
(45) Joanny, J. F.; Leibler, L.; Ball, R. *J. Chem. Phys.* **1984**, *81*, 4640. Schäfer, L.; Kappeler, Ch. *J. Phys. (Paris)* **1985**, *46*, 1853.
(46) Broseta, D.; Leibler, L.; Joanny, J. F. *Macromolecules* **1987**, *20*, 1935.
(47) Bates, S. F.; Muthukumar, M.; Wignall, G. D.; Fetters, L. J. *J. Chem. Phys.* **1988**, *89*, 535.
(48) Dudowicz, J.; Freed, K. F. *Macromolecules* **1991**; *Macromolecules*, submitted. Dudowicz, J.; Freed, M. S.; Freed, K. F. *Macromolecules*, in press.
(49) Brereton, M.; Vilgis, T. *J. Phys. (Paris)* **1989**, *50*, 245. Vilgis, T.; Borsali, R. *Macromolecules* **1990**, *23*, 3972.
(50) Schweizer, K. S.; Curro, J. G. *Phys. Rev. Lett.* **1988**, *60*, 809; *J. Chem. Phys.* **1988**, *88*, 7242; *J. Chem. Phys.* **1989**, *91*, 5059. Schweizer, K. S.; Curro, J. G. *J. Chem. Phys.* **1991**, *94*, 3986.
(51) Schweizer, K. S.; Curro, J. G. *Chem. Phys.* **1990**, *149*, 105. Curro, J. G.; Schweizer, K. S. *Macromolecules* **1990**, *23*, 1402; **1991**, *24*, 6736.
(52) Lipson, J. E. G. *Macromolecules* **1991**, *24*, 1334.
(53) Binder, K. In *Computer Simulation Studies in Condensed Matter Physics*; Springer Proceedings in Physics, Vol. 33; Landau, D. P., Mon, K. K., Schüttler, H.-B., Eds.; Springer: Berlin, 1988; p 84.
(54) Sariban, A.; Binder, K., to be published.
(55) Sariban, A.; Binder, K. *Macromol. Chem.* **1988**, *189*, 2357. Sariban, A. *Macromolecules* **1991**, *24*, 578.
(56) Carmesin, I.; Kremer, K. *Macromolecules* **1988**, *21*, 2819; *J. Phys. (Paris)* **1990**, *51*, 915.
(57) Wittmann, H. P.; Kremer, K. *Comput. Phys. Commun.* **1990**, *61*, 309.
(58) Deutsch, H.-P.; Dickman, R. *J. Chem. Phys.* **1990**, *93*, 8983.
(59) Deutsch, H.-P.; Binder, K. *Chem. Phys.* **1991**, *94*, 2294.
(60) Paul, W.; Binder, K.; Heermann, D. W.; Kremer, K. *J. Phys. (Paris)*. **1991**, *111*, 37; *J. Chem. Phys.*, in press.
(61) Ferrenberg, A. M.; Swendsen, R. H. *Phys. Rev. Lett.* **1988**, *61*, 2635; *Phys. Rev. Lett.* **1989**, *63*, 1195.
(62) Fisher, M. E. In *Critical Phenomena*; Green, M. S., Ed.; Academic Press: New York, 1971; p 1. Privman, V., Ed. *Finite Size Scaling and Numerical Simulation of Statistical Systems*; World Scientific: Singapore, 1990.
(63) Barber, M. N. In *Phase Transitions and Critical Phenomena*; Domb, C., Lebowitz, J. L., Eds.; Academic Press: New York, 1983; Vol. 8, p 157.
(64) Binder, K. Z. *Phys. B* **1981**, *43*, 119; *Ferroelectrics* **1987**, *73*, 43.
(65) Deutsch, H.-P. *J. Stat. Phys.* **1992**, *67*, 1039; Dissertation, Johannes Gutenberg-Universität Mainz, 1991, unpublished.
(66) Very brief accounts of a few of these data were presented in: Deutsch, H.-P.; Binder, K. *Europhys. Lett.* **1991**, *17*, 697; *Polym. Prepr. (Am. Chem. Soc., Div. Polym. Chem.)* **1991**, *32*, 499.
(67) Schwahn, D.; Mortensen, K.; Yee-Madeira, H. *Phys. Lett.* **1987**, *58*, 1544.
(68) Bates, S. F.; Rosedale, J. H.; Stepanek, P.; Lodge, T. P.; Wiltzius, P.; Fredrickson, G. H.; Hjelm, R. P., Jr. *Phys. Rev. Lett.* **1990**, *65*, 1893.
(69) Chu, B., private communication.
(70) Meier, G.; Momper, B.; Fischer, E. W. Preprint, 1991.
(71) Shibanov, Yu. D.; Komaricheva, L. I. *Pis'ma Zh. Eksp. Teor. Fiz.* **1990**, *51*, 409.
(72) Hohenberg, P. C.; Halperin, B. I. *Rev. Mod. Phys.* **1977**, *49*, 435.
(73) Binder, K.; Heermann, D. *Monte Carlo Simulation in Statistical Physics. An Introduction*; Springer: Berlin, 1988.
(74) Chestnut, D. A.; Salsburg, Z. W. *J. Chem. Phys.* **1963**, *38*, 2861.
(75) Le Guillou, J. C.; Zinn-Justin, J. *Phys. Rev. B* **1980**, *21*, 3976.
(76) Ginzburg, V. L. *Sov. Phys. Solid State* **1960**, *2*, 1824.
(77) Fisher, M. E. *Rev. Mod. Phys.* **1974**, *46*, 597.
(78) Gunton, J. D.; San Miguel, M.; Sahni, P. S. In *Phase Transitions and Critical Phenomena*; Domb, C., Lebowitz, J. L., Eds.; Academic: New York, 1983; Vol. 8, p 267.
(79) Binder, K. *Rep. Progr. Phys.* **1987**, *50*, 783.
(80) Chu, B.; Schoenes, F. J.; Fisher, M. E. *Phys. Rev.* **1969**, *185*, 219.
(81) Bates, S. F.; Muthukumar, M.; Wignall, G. D.; Fetters, L. J. *J. Chem. Phys.* **1988**, *89*, 535.
(82) Joyce, G. S. In *Phase Transitions and Critical Phenomena*; Domb, C., Green, M. S., Eds.; Academic: New York, 1972; Vol. 2, p 375.
(83) We are deeply indebted to Prof. K. Schweizer for clarifying correspondence on this point.
(84) Ferrenberg, A.; Landau, D. P. *Phys. Rev. B* **1991**, *44*, 5081.
(85) Binder, K.; Nauenberg, M.; Privman, V.; Young, A. P. *Phys. Rev. B* **1985**, *31*, 1498.
(86) In ref 41 the response function was defined not with respect to the chemical potential difference μ per chain, as done here, but with respect to the chemical potential difference $\Delta\mu$ per monomer. Since obviously $\mu = N\delta\mu$, this introduces an additional power of N in equations corresponding to eqs 56 and 57. We here choose the present, different notation since it more clearly displays the fact that all these singular amplitude dependences (eqs 55–59) are linked to the distinction between the critical exponent of each quantity $\{\beta, 1/\delta, \gamma, \gamma/(\beta\delta), ...\}$ and its corresponding mean-field value $\{1/2, 1/3, 1, 3/2, ...\}$.
(87) Budkowski, A.; Steiner, U.; Klein, J.; Schatz, G. Preprint of Coexistence in polymer mixtures.
(88) Privman, V.; Aharony, A.; Hohenberg, P. C. In *Phase Transitions and Critical Phenomena*; Domb, C., Lebowitz, J. L., Eds.; Academic: New York, 1991; Vol. 14.